

## Mineralogical assemblages, geochemistry and fossil associations of Pleistocene–Holocene complex siliciclastic deposits from the Southwestern Doñana National Park (SW Spain): A palaeoenvironmental approach

Manuel Pozo <sup>a,\*</sup>, Francisco Ruiz <sup>b</sup>, María Isabel Carretero <sup>c</sup>, Joaquín Rodríguez Vidal <sup>b</sup>, Luís Miguel Cáceres <sup>b</sup>, Manuel Abad <sup>b</sup>, María Luz González-Regalado <sup>b</sup>

<sup>a</sup> Departamento de Geología y Geoquímica, Universidad Autónoma de Madrid, 28049-Madrid, Spain

<sup>b</sup> Departamento de Geodinámica y Paleontología, Universidad de Huelva. Avda. Fuerzas Armadas, s/n. 21071-Huelva, Spain

<sup>c</sup> Departamento de Cristalografía, Mineralogía y Química Agrícola, Universidad de Sevilla, Apdo. 553, Sevilla, Spain

### ARTICLE INFO

#### Article history:

Received 30 September 2009

Received in revised form 11 January 2010

Accepted 22 January 2010

Available online 1 February 2010

Communicated by M.R. Bennett

#### Keywords:

Estuarine environment

Tsunami

Quaternary

Clay mineralogy

Geochemistry

### ABSTRACT

On the basis of mineralogy, chemical and palaeontological data collected in a long core (93 m) three associations of facies are distinguished in the Late Pleistocene–Late Holocene evolution of the sedimentary infilling in nowadays Doñana National Park. From the lower, middle and upper associations of facies three sedimentological phases have been established. In the oldest phase (>44 kyr BP), this area was occupied by supratidal, freshwater marshes located close to a brackish lagoon and inundated suddenly by brackish-marine inputs. The following phase (44–7 kyr BP) is characterized by the transition from supratidal to intertidal conditions, with the alternation of freshwater or brackish marshes situated very close or in the margin of the former lagoon and submitted to episodes of desiccation or tidal inundation. The last phase (7–3.0 cal kyr BP) comprised: a) a marine inundation during the maximum of the Flandrian transgression (~7–6.5 cal kyr BP); and b) the progressive infilling of a brackish lagoon with marine connection and permanent fresh water inputs (6.5–3.5 cal kyr BP), partially enclosed by the Doñana spit. The phyllosilicate-rich, clayey-silty sequence of this latter infilling is interrupted by tsunami-like deposits at 4.2–3.6 cal kyr BP and 3.6–3.0 cal kyr BP. These high-energy events are characterized by textural (bimodal grain-size distribution, sorting decrease), mineralogical (crystallochemical changes in illites, increasing dolomite content) and geochemical changes (Ti anomaly), besides a sudden introduction of marine bivalves and microfauna and a strong decrease or the almost disappearance of the brackish ostracode assemblage. Ages of these deposits coincide with those indicated for other tsunamigenic layers detected in the southwestern Spanish coasts and some deep cores collected near the African–European plate boundary.

© 2010 Elsevier B.V. All rights reserved.

### 1. Introduction

The Pleistocene–Holocene evolution of estuaries, deltas, lagoons or the associated salt marshes have received an increasing attention in the last two decades (De la Vega et al., 2000; Edwards, 2001; Gerdes et al., 2003; Canali et al., 2007). The main palaeoenvironmental changes have been deduced from the multidisciplinary analysis of the geological record contained in several continuous cores. They include usually vertical lithostratigraphical, mineralogical and isotopic data as key tools to determine the origin and evolution of sediments, the variations of some physical–chemical water parameters or even palaeoclimatic oscillations (Chamley, 1989; Skrabal, 1991; Carretero et al., 2002; Reeves et al., 2007). The use of carbonate stable isotopes

for the interpretation of depositional environments relies upon the characteristic of some chemical, biological and mechanical processes to fractionate stable isotopes as a result of the relative bond energies (Mason and Surdam, 1992). Moreover, the fractionation of  $\delta^{18}\text{O}$  is dependent upon the composition of the original waters and the depositional environment (Anderson and Arthur, 1983).

Results derived from these investigations are contrasted with those derived from the palaeontological record in order to obtain either a detailed analysis of a short time interval or several successive palaeogeographic reconstructions along a longer period (Grauert et al., 2001; Vött et al., 2006). In addition, several groups of microfossils (diatoms, foraminifers, ostracodes, calcareous nannoplankton, and pollen) have been used as tracers of the main palaeoenvironmental features (Cearreta et al., 2003; Fontana, 2005; Zong et al., 2006; Bao et al., 2007). The final interpretations can be improved if additional macrofossil groups are studied and the (palaeo-)autoecology of their main assemblages is taken into account (Hayward et al., 2002; Compton, 2007).

\* Corresponding author. Tel.: +34 91 4974808.

E-mail address: [manuel.pozo@uam.es](mailto:manuel.pozo@uam.es) (M. Pozo).

In this general scenario, it is the frequent presence of distinctive sedimentary layers with characteristic textural and mineralogical features that have been attributed to storms, cyclones, hurricanes or tsunamis (Clague et al., 2000; Singarasubramanian et al., 2006; Tripsanas et al., 2007). These special beds usually show a palaeontological record that differentiates them from the underlying sediments (Luque et al., 2002; Kontopoulos and Avramidis, 2003; Wagner et al., 2007).

In this paper, we perform an integrated geological study of a continuous core, collected in the southwestern part of the Doñana National Park (Guadalquivir estuary, SW Spain), using lithostratigraphic, mineralogical, geochemical and palaeontological analyses, together with radiocarbon datings and isotopic data. On the basis of mineralogical assemblages, major elements trend, fossil content and stable isotope data the main aim is to establish the environmental changes occurring during the Late Pleistocene–Holocene period in this area.

## 2. Materials and methods

### 2.1. Study area and sampling

The Doñana National Park is one of the largest wetlands (50,720 ha) in Europe, located in southwestern Spain where the Guadalquivir River is partly blocked in the lower reach by sandy barriers, resulting in a large estuary (1800 km<sup>2</sup>). The sedimentary deposits infilling the studied zone are mainly fine-grained siliciclastic facies (clayey silts to silts) with local inserts of relative coarser grained facies (sandy silts to silty sands) (Pozo et al., 2008). Besides the presence of fluvial levees flanking the river and its former courses, common features are bioclastic and sandy ridges, depressions occupied by small freshwater ponds and sandy spits (Fig. 1). The sampling has been done in a long core (PLN) drilled by the Spanish Geological and Mining Institute (IGME) in the southwestern part of the Doñana National Park, close to the so-called 'Palacio de las Nuevas'. The studied lithological section has a thickness of 93 m

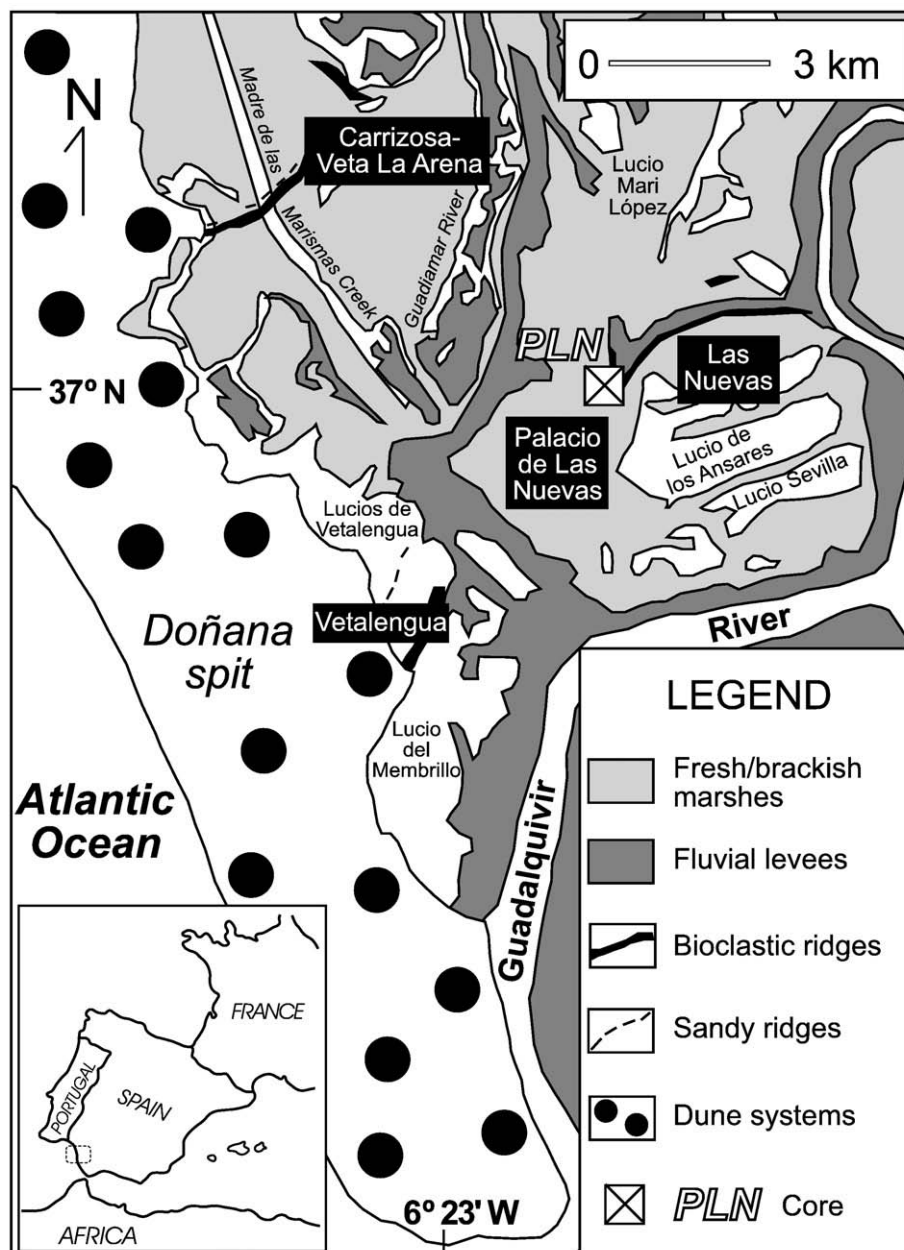


Fig. 1. Geographical setting and geomorphology of the Guadalquivir River mouth. The location of the core PLN within the Doñana marshlands is also shown.

composed mainly of fine-grained siliciclastic lithofacies overlying coarse to very coarse sands with subrounded gravel inserts. Twenty eight samples have been collected for textural, mineralogical, geochemical and palaeontological analyses.

## 2.2. Textural and compositional analysis

Owing to the predominance of detrital facies, the lithological description has been complemented with grain-size analysis of the entire collected samples. Grain-size distribution was determined by wet sieving for the coarser fractions (> 100 µm). Fractions lesser than 100 µm were analyzed by photosedimentation (MicromeriticsR SediGraph 5100 ET). Na-hexametaphosphate has been used as a dispersing agent.

The mineralogical analysis of the samples was carried out by means of X-ray diffraction (XRD) using a SIEMENS D-5000 equipment with a scanning speed of 1° 2θ/min and Cu-Kα radiation (40 kV, 20 mA). XRD studies were carried out both on randomly oriented samples (total fraction) and selected clay fraction samples (<2 µm). Powdered (<63 µm) whole-rock samples were scanned from 2° to 65° 2θ. Clay fraction samples were prepared from cation-saturated, ultrasonic treated suspensions oriented on glass slides. The identification of the clay fraction minerals was carried out on oriented Mg<sup>2+</sup>-saturated samples with ethylene glycol solvation, and also after heating at 550 °C following K<sup>+</sup> saturation. Quantitative estimation of the mineral content was carried out using the intensity factors calculated by Schultz (1964) and Barahona (1974).

Selected undisturbed samples were slightly coated with gold and examined with a PHILIPS SEM XL-30 electron microscope equipment with EDX analytical system. In addition, the medium to fine sand fraction (0.10 mm–0.25 mm) of 12 samples was examined under the optical microscope to recognize the presence of heavy minerals.

With the aim of confirming the mineralogical results and achieving a more accurate identification of the minerals contained in the complex siliciclastic facies the chemical analysis of major elements of twenty seven samples was carried out. The chemical analysis of Si, Al, Ca, K, Mg, Fe, P and Ti was performed by means of the MagiX X-ray fluorescence (XRF) spectrometer of PANalytical. A Varian 220-FS QU-106 atomic absorption (AA) spectrophotometer was used for the determination of Na.

## 2.3. Palaeontology

The macrofossil record of 28 sub-samples was obtained by washing the bulk sediment (12 cm<sup>3</sup>) through a 1-mm sieve. Bivalves and gastropods were identified to the species level and counted to study the semi-quantitative distribution in the core. In relation to the reduced amount of sediment studied, the abundance of a species in each sample was described as follows: rare (1–5 specimens), frequent (6–15 specimens) and abundant (>15 specimens). The semi-quantitative abundance of other groups (bryozoans, characeans, diatoms, miliolids and planktonic foraminifers) and spines of echinoderms was also calculated in the same way.

In addition, sub-samples of approximately 15 g were selected for microfossil analysis. These sub-samples were washed through a 63-µm sieve to remove the mud fraction and then dried. If possible, more than 300 ostracode valves and carapaces from each sample were picked onto faunal microscope slides. Both the abundance of each species (rare: <10 specimens; frequent: 10–100 specimens; abundant: 101–500 specimens; very abundant: >500 specimens) and the number of individuals per gram in each sample was calculated.

## 2.4. Isotopic analysis

A total of 12 samples of sediments have been chosen for isotopic analysis, all of them consisting of calcite and/or dolomite. The low content of dolomite in some samples (<10%) provoked that only 9

samples were analyzed for this mineral. Samples for isotopic analysis were taken carefully by means of stereomicroscope examination avoiding shell remains or other calcareous bioclasts.

Oxygen and carbon stable isotope measurements were carried out in the Stable Isotope Laboratory of the Salamanca University, Spain. There were 12 samples ground to pass through a 100-mesh sieve, whereas the 250-mesh fraction was saved for analysis of both oxygen and carbon isotopes. The fractionated extraction of CO<sub>2</sub> from carbonates for isotope analysis followed standard techniques (McCrea, 1950; Craig, 1957). For isotope analysis calcite and dolomite were reacted with phosphoric acid at 25 °C. All samples were prepared and analyzed at least in duplicate. The analytical precision is generally ±0.1‰ for carbon and ±0.15‰ for oxygen. Both the oxygen and carbon values were initially reported in δ ‰ relative to PDB.

## 2.5. Radiocarbon chronology

Five dates were produced at the Beta Analytic Laboratory (Miami, USA) by radiocarbon analysis of mollusc shells (Table 1). Four of them were calibrated using CALIB version 5.0.1 (Stuiver and Reimer, 1993) and the Stuiver et al. (1998) calibration dataset. The final results correspond to calibrated ages using 1σ–2σ intervals, with the reservoir corrections suggested by Soares (2008) for this area.

## 3. Results

### 3.1. Lithofacies, mineralogy and major elements geochemistry

From a sedimentological point of view three facies associations, including ten lithostratigraphic units, have been differentiated (Fig. 2). The lithostratigraphic analysis is based on hand sample description, texture (grain-size distribution) and composition (both mineralogy and major elements geochemistry). On the basis of sand, silt and clay content different lithofacies have been established, according to Folk's (1980) classification. The ternary graphic and grain-size distributions of representative samples from the different units are shown in Fig. 3.

#### 3.1.1. Lower facies association (LFA)

**3.1.1.1. Lithostratigraphy.** This association consists of three lithostratigraphic units. Unit I (–93 to –74 m) is represented by a continuous sequence of silts with limited sand contents (<9%) and very rare fragments of bivalves. Color shows a gradual transition from the basal reddish to the upper greenish–greyish shades (5GY8/1). These fine-grained sediments present thin parallel lamination. Unit II (–74 to –69 m) is formed by friable massive greyish to yellowish (5Y8/4) silty sands. The base of the overlying Unit III (–69 to –59 m) presents an alternation of both silty and clayey layers with a very fine thickness (5–20 cm), only interrupted by a friable greyish yellow (5Y8/4) sandy insert (–63 to –62.7 m). At top of this unit, yellowish grey (5Y7/2) massive muds (up to 30% clay) display reddish iron stains coating vertical fissures. The representative grain-size distributions of these three units are shown in Fig. 3.

**Table 1**  
Database of <sup>14</sup>C results.

Core-depth (cm)	Lab. number	<sup>14</sup> C age (BP)	Error	cal BP (1σ)	cal BP (2σ)
PLN-30	B-228880	3550	40	3457–3192	3590–3033
PLN-1080	B-228881	4060	40	4114–3817	4269–3665
PLN-1410	B-228885	4200	40	4295–3984	4428–3847
PLN-2610	B-228882	6090	40	6733–6619	6789–6543
PLN-5530	B-228883	43,370	960	Uncalibrated	

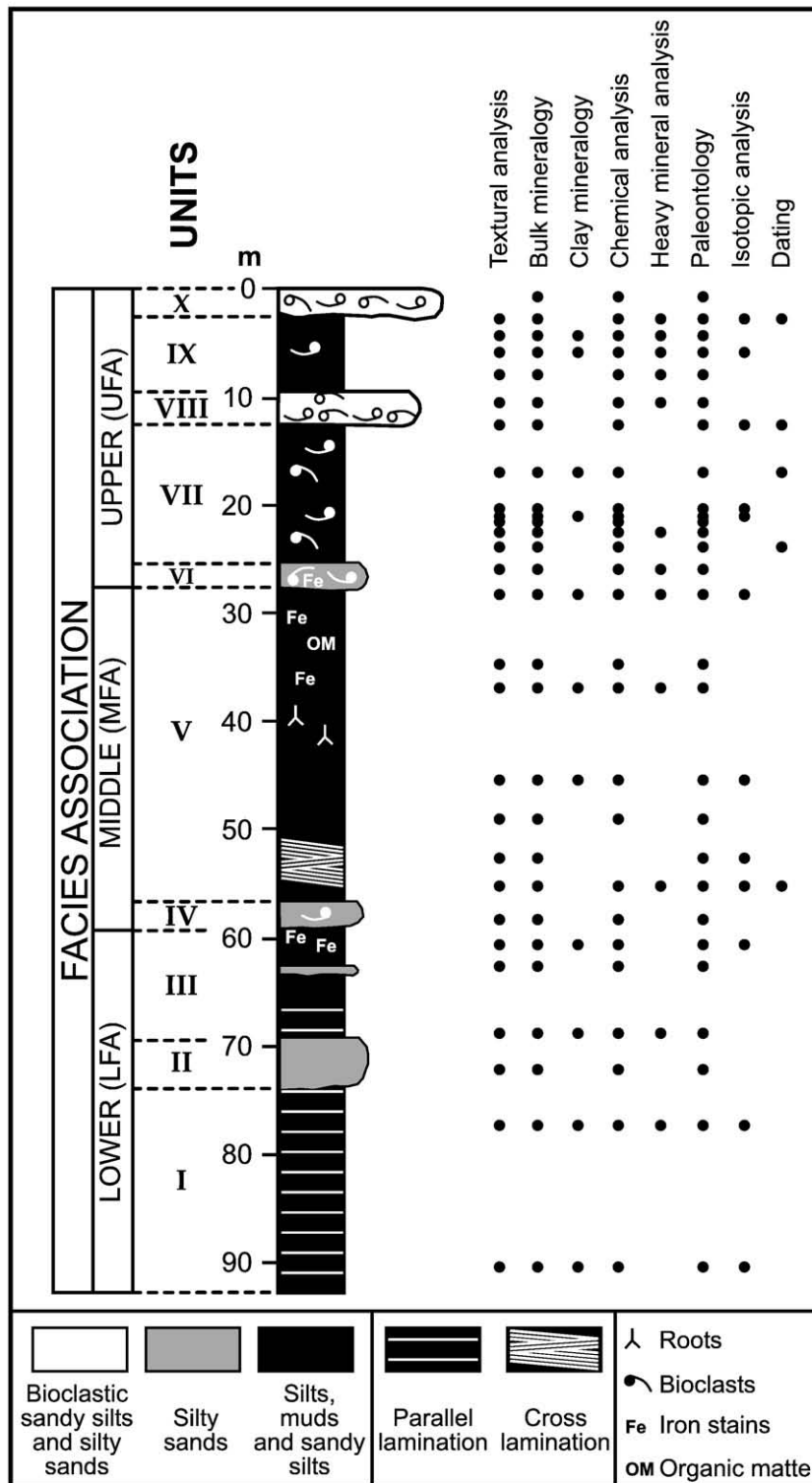


Fig. 2. Lithostratigraphic section showing the location of the studied samples and the different analyses carried out.

3.1.1.2. *Mineralogical assemblages.* The relative more fine-grained sediments (Units I and III) show a mineralogical composition dominated by phyllosilicates (40–65%; mean 51%), with calcite as main carbonate (10–30%; mean 20%) and scarce dolomite (<10%; mean 7%). The abundance of quartz and feldspars (both plagioclase and potassium feldspar) is lower than 15%, although exceptionally feldspars can reach 25% (mainly potassium feldspar) in sandy-mud laminated sediments (Fig. 4). The thin sandy-silt insert of Unit III is

characterized by its enrichment in dolomite content (20%) with calcite rounding 15%, whereas quartz and feldspars show low contents (<15%) and phyllosilicates achieve 45% of the total mineralogy. Under the SEM examination dolomite occurs as angular detrital grains (Fig. 5a) suggesting inherited origin.

Compared with the underlying fine-grained sediments, Unit II displays an increase in quartz and feldspars (potassium feldspar > plagioclase), reaching 39% and 13%, respectively. On the other hand, a

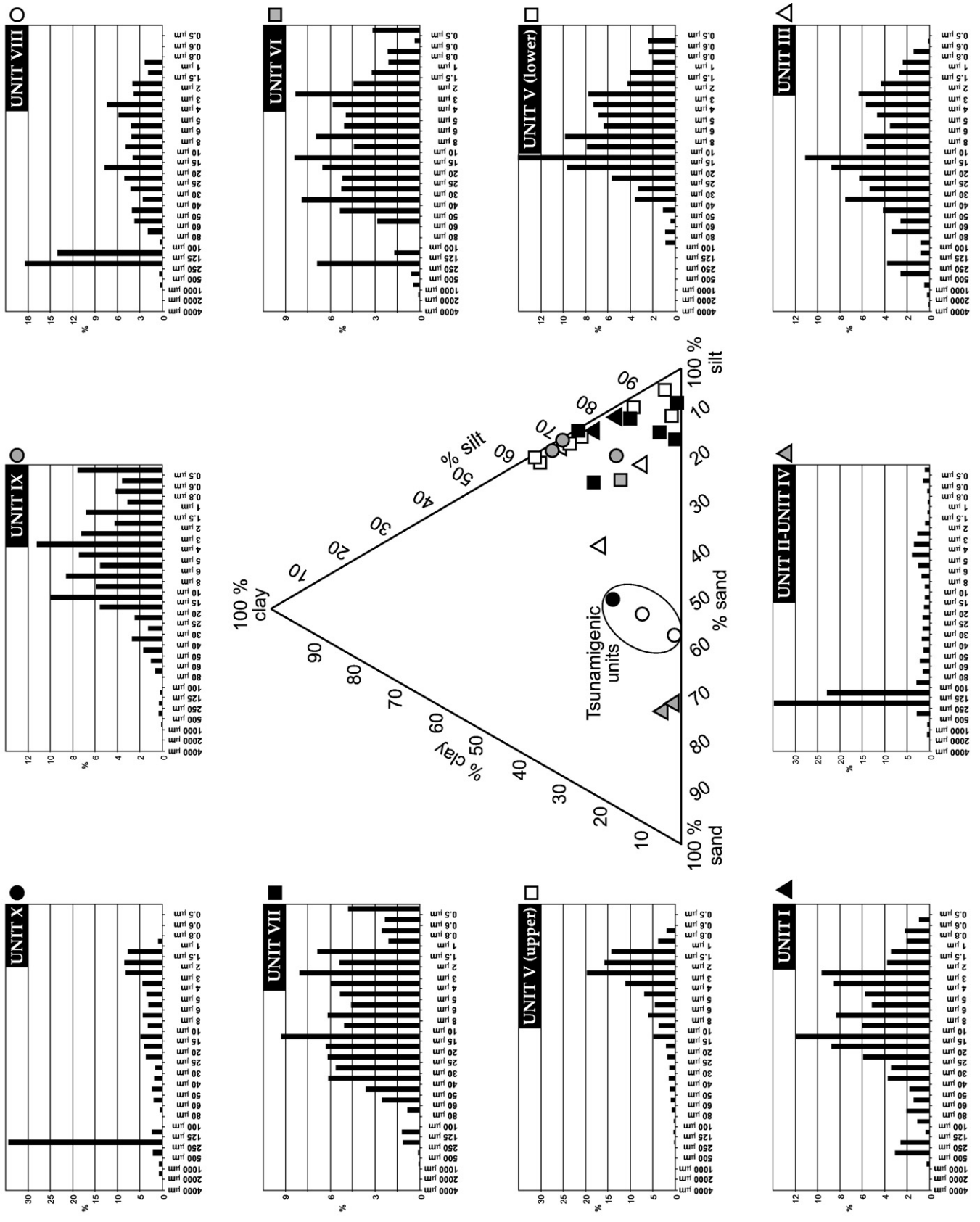


Fig. 3. Textural composition and grain-size distribution. The histograms belong to representative facies of the core PLN. Samples from tsunamigenic unit are encircled.

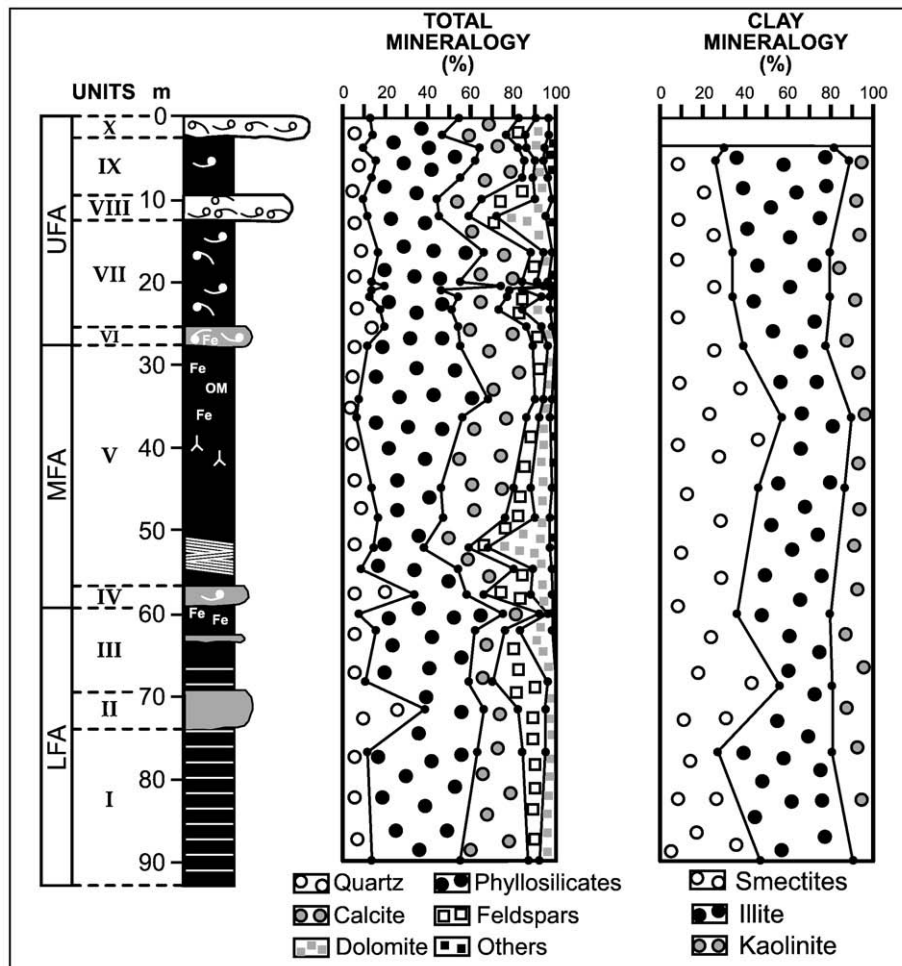


Fig. 4. Mineralogy of bulk and clay fractions along the PLN core. Others comprise halite, gypsum and aragonite.

lower abundance of phyllosilicates (<30%), calcite and dolomite (lower than 20% together) has been observed.

Heavy minerals of these units are represented by garnet and rutile with subordinated hornblende, pyroxene, opaques and staurolite. In addition, metamorphic rock fragment grains have been recognized in these three units.

**3.1.1.3. Clay mineralogy.** Illite (mean 42%) and smectite (mean 40%) predominate in this lower association, ranging between 25 and 56% (Fig. 4). The increase of illite and kaolinite contents is concurrent, especially close to more detrital beds. Traces of random mixed layers (mostly 10–14 Å) have been identified.

Regarding smectites the Biscaye index is low (<0.2) with scarce vertical variation, and as well as kaolinite (11–23%) shows a content increase from the bottom to the top. Illite displays 002/001 ratios between 0.38 and 0.51 with a mean value of 0.43, and a growing trend toward the top. Illite crystallinity (FWHM) fluctuates between 0.31 and 0.54 ( $2\theta$ ) with a crystallite size ranging from 16 to 23 nm.

The low Biscaye index of smectites is reliable with a poor ordering and the presence of randomly mixed layers illite–smectite, this fact seems to be related to weathering processes (non-confined milieu) affecting reworked soils.

The clay mineral assemblage is interpreted as inherited and its distribution controlled by detrital inputs but also for the different behaviour for settling/flocculation in saline waters.

**3.1.1.4. Geochemistry.** Significant variations in major element abundances (expressed as oxides) have been observed (Fig. 6). The  $\text{SiO}_2$

content is always above 40%, the higher values observed of all the studied samples. Silica concentrates especially in coarse-grained sediments (>62%), whereas  $\text{Na}_2\text{O}$  and  $\text{K}_2\text{O}$  contents exhibit a slight increase in these layers coinciding with a noteworthy decline of all the other elements. These results are coincident with the mineralogy where a remarkable increase of quartz is observed (e.g., sample PLN-3).

The abundance of  $\text{Al}_2\text{O}_3$  and  $\text{CaO}$  shows limited variation (<15%), anyway  $\text{CaO}$  shows the lowest contents of the whole core. Some oxides ( $\text{Fe}_2\text{O}_3$ ,  $\text{TiO}_2$ , and  $\text{MnO}$ ) display the same behaviour in these units, with the two last reaching the highest contents of the borehole. Regarding  $\text{Fe}_2\text{O}_3$  the higher content is showed in fine-grained sediments, with some exception in Unit III. This relatively thin insert of sandy silts include iron (hydr)oxides stains, giving explanation for  $\text{Fe}_2\text{O}_3$  contents up to 5%. Likewise the identification by means of SEM–EDX of Ti-rich strongly altered silicate grains justifies the  $\text{TiO}_2$  anomaly observed (Fig. 5b). In addition,  $\text{P}_2\text{O}_5$  shows a similar trend to above mentioned elements, but an anomalous increase (0.21%) – the highest of all samples – has been observed near the top of Unit III.

### 3.1.2. Middle facies association (MFA)

**3.1.2.1. Lithostratigraphy.** This association comprises two lithostratigraphic units. Unit IV (–59 to –57 m) is composed of dark pale yellowish brown (10YR6/2) silty sands, with some ochre to reddish iron-rich nodules and scattered fragments of bivalves. The representative grain-size distribution is shown in Fig. 3.

Unit V (–57 to –27.5 m) consists of greyish orange silts (10YR7/4) to greenish or yellowish grey (5Y8/1–10Y8/2) silts to muds, with very

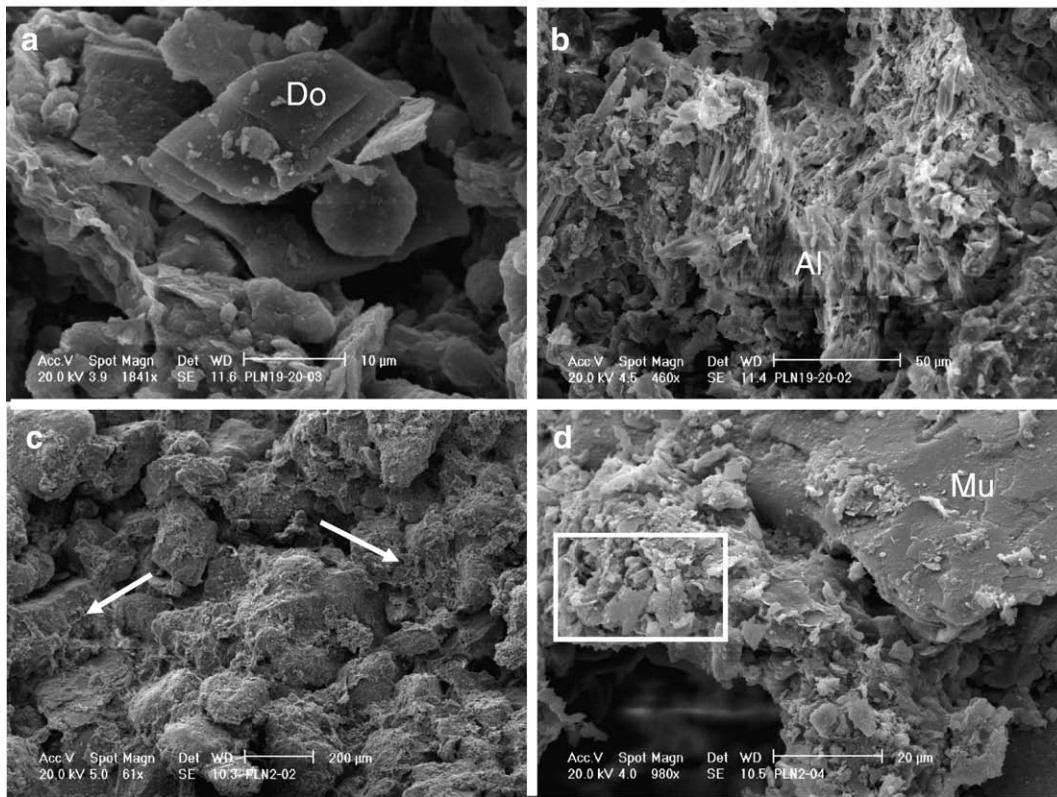


**Fig. 5.** SEM images. a) Detail of detrital dolomite grain (Do) in sandy-silt insert from Unit III (LFA). b) Altered ferromagnesian grain (Al) in sandy-silt insert from Unit III (LFA), highlighting the content in iron and titanium. (EDX: 41.87% SiO<sub>2</sub>, 25.85% Fe<sub>2</sub>O<sub>3</sub>, 13.85% MgO, 11.56% CaO, 5.38% TiO<sub>2</sub>, 1.49% K<sub>2</sub>O). c) Clastic texture of sample PLN-27 (Unit X, UFA) displaying a chaotic distribution of silt-clay particles (arrows), coating, infilling and bridging poorly sorted sand grains. d) Detail of sample PLN-27 showing the presence of micaceous minerals (muscovite) both in skeletal grains (Mu) and silty clay matrix (white box).

low sandy contents (Fig. 3: <2%) and increasing clay percentages (14–34%) toward the top. This is a complex unit highlighting cross lamination in slightly sandy-silt levels at the base passing upward to a distinct dark level (5GY6/1) showing root/plant remains and massive greenish clayey silts with common iron stains.

**3.1.2.2. Mineralogical assemblages.** Unit IV shows an outstanding increase in quartz and feldspars (plagioclase > potassium feldspar) in comparison with Unit III, reaching 34 and 23%, respectively (Fig. 4). The sudden decrease in phyllosilicate abundance (24%) and the low content of calcite and dolomite (about 10%) is noteworthy.

Phyllosilicates display two peaks in Unit V, one at the base (45%) and the other near the top (65%), respectively. In these muddy beds the content in quartz and feldspars is low (<10%) and calcite (23–33%) is predominant over dolomite (<10%). In addition, the silty sediments show a lower phyllosilicate content (<30%), but they are enriched in quartz (15%) and feldspars (10%). Within phyllosilicates, muscovite has been identified in all units, but also paragonite in Unit V.

Concerning carbonates, calcite is predominant (20–35%) over dolomite (<15%), except in sample PLN-9 (dolomite > 30%). In addition, the first identification of gypsum (<5%) is remarkable.

Heavy mineral assemblage is represented by garnet, titanite, zircon, hornblende and rutile with subordinated kyanite, andalusite, hematite, chlorite and opaques (Fig. 7a, d). In all the units the presence of metamorphic rock fragment grains has been observed. The high content in carbonized root plant debris, often displaying cellular textures is also remarkable.

**3.1.2.3. Clay mineralogy.** Smectite is the main clay mineral (>56%) in Unit V, followed by illite (31–41%; mean 37%) and kaolinite (11–23%;

mean 16%). Kaolinite content shows an opposite trend to smectite, increasing at the top (Fig. 4). Traces of random mixed layers (mostly 10–14 Å) have been identified.

Concerning smectite, the Biscaye index is low to moderate (0.14–0.31) reaching the highest value in the most smectitic samples. On the other hand, the behaviour of illite is akin to kaolinite, displaying 002/001 ratios between 0.26 and 0.31 (mean value 0.29) lower than previous assemblages, indicating illite enrichment in Mg and Fe with respect to Al in octahedral sheet. Illite crystallinity (FWHM) fluctuates between 0.38 and 0.55 (2 $\theta$ ) with a crystallite size ranging from 16 to 23 nm. An opposite trend between illite content and crystallinity has been observed.

Clay mineral assemblage is similar to that reported in LFA, but in this case the smectite order (Biscaye index) is higher, indicating conditions of more stability for smectite in the sedimentary environment.

**3.1.2.4. Geochemistry.** The behaviour of both CaO and dolomite is not meaningful, although their contents are higher than reported in the lower facies association. On the other hand, silica shows higher percentages in Unit IV and decrease with TiO<sub>2</sub> upward in Unit V, coinciding with an increase of MnO and the lower values of Al<sub>2</sub>O<sub>3</sub>, K<sub>2</sub>O, P<sub>2</sub>O<sub>5</sub> and Fe<sub>2</sub>O<sub>3</sub>. P<sub>2</sub>O<sub>5</sub> reaches the lowest value in root bioturbated sediments, whereas Fe<sub>2</sub>O<sub>3</sub> presents the highest contents in the basal clayey silts of this unit, where abundant (hydr)oxide stains are reported.

Some correlation was found between oxide contents and grain size. Percentages of Al<sub>2</sub>O<sub>3</sub> and K<sub>2</sub>O decrease in silty samples of Unit V, but increase together with SiO<sub>2</sub> and Fe<sub>2</sub>O<sub>3</sub> in clayey silts. In addition, silts from this unit show the highest content in MgO, decreasing upward in muds. This trend correlates well with the dolomite abundance.

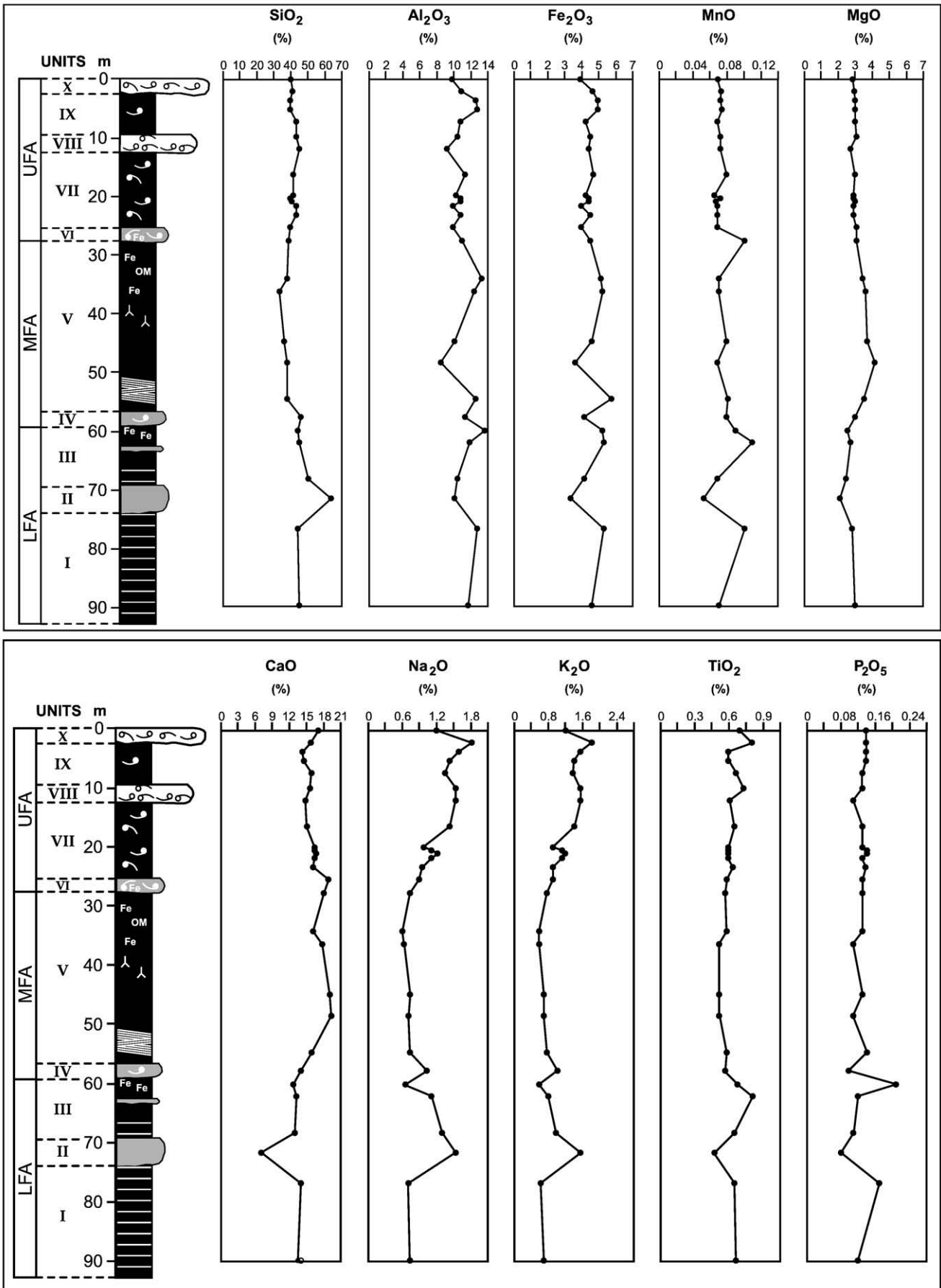


Fig. 6. Geochemical evolution of major elements along the PLN core.

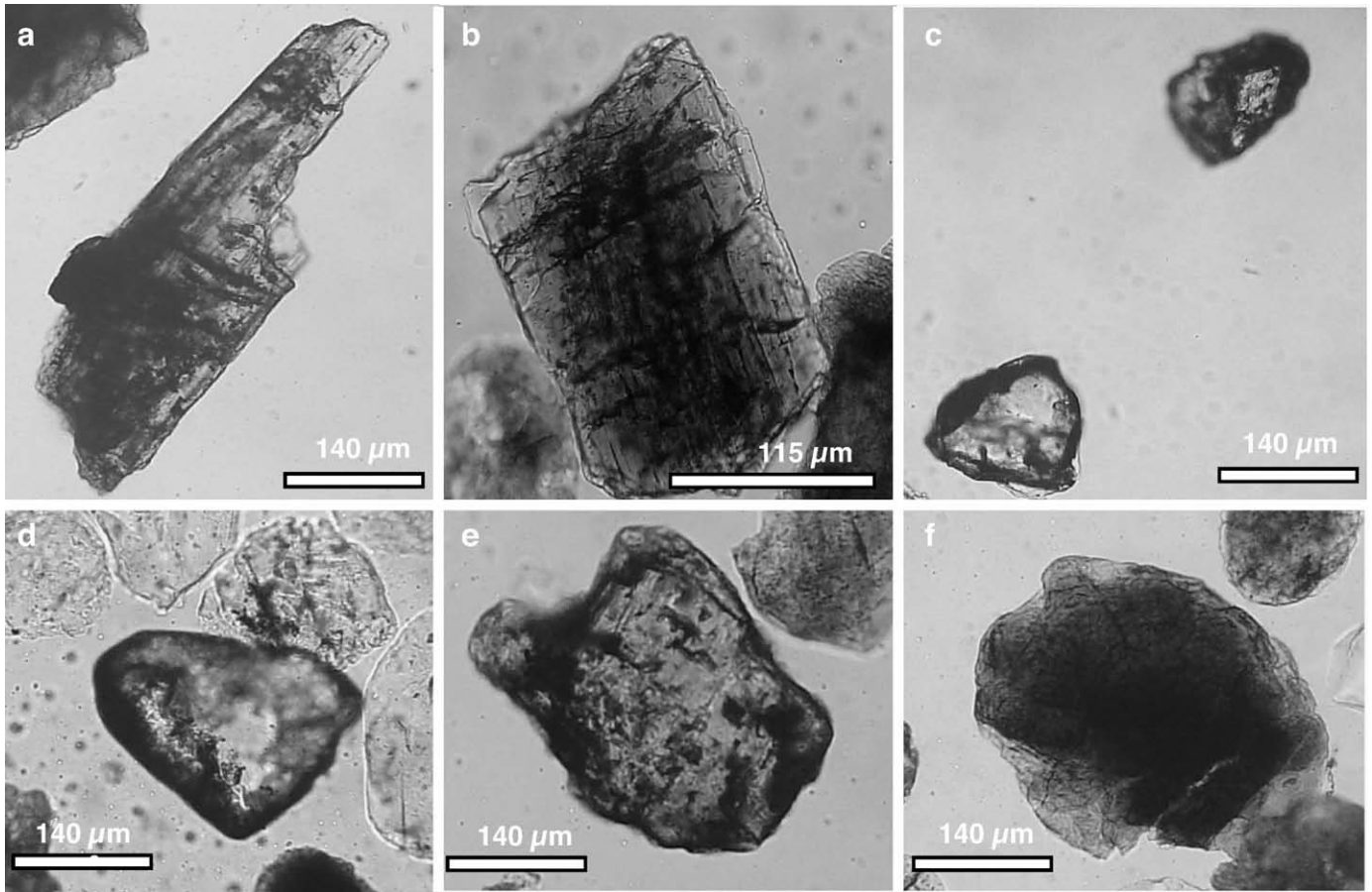


Fig. 7. Representative heavy minerals. a) Kyanite (PLN-14) N//. b) Hornblende (PLN-24) N//. c) Garnet (PLN-14) N//. d) Zircon (PLN-24) N//. e) Rutile (PLN-24) N//. f) Chlorite (PLN-27) N//.

### 3.1.3. Upper facies association (UFA)

**3.1.3.1. Lithostratigraphy.** This association comprises five lithostratigraphic units. Unit VI (–27.5 to –26 m) is constituted by two fine layers of dark, greyish (10YR6/2) clayey–sandy silts with ochre limonite stains and frequent carapaces of gastropods. The following 14.6 m (Unit VII) are characterized by muds (Fig. 3: silts + clays > 96%), with some interbedded sandier levels (e.g., –21.4 to –21.3 m). This unit presents a gradual transition from dark greyish (5Y7/2) to brighter, greenish (10YR5/3) shades toward the top. Carapaces and fragments of molluscs are frequent accounting for a gravel content of 7%, except in the upper 2 m.

Unit VIII (–11.4 to –9.3 m) is represented by yellowish to greyish brown (10YR6/2) sandy silts to silty sands with scarce shells and fragments of bryozoans. This unit includes a basal, fine level (–11.4 to –11.2 m) of fine silty sands, characterized by very numerous fragmented shells (up to 2.6% gravel).

Unit IX (–9 to –1.8 m) is composed of a monotonous sequence of greenish to dark yellowish brown (10YR4/2) muds to silts with decreasing sandy percentages (9.5–1.2%) toward the top. The uppermost 1.8 m (Unit X) consists of greyish to dark yellowish brown (10YR4/2) silty sands to sandy silts (Fig. 3: sands ~43%; silts ~40%) with abundant disarticulated valves and fragments of bivalves, together with frequent carapaces of gastropods.

**3.1.3.2. Mineralogical assemblages.** The passing of clayey–sandy silts of Unit VI toward silts of Unit VII displays a noteworthy increase of phyllosilicates and feldspars (potassium feldspar > plagioclase), whereas quartz decrease slightly (Fig. 4). Concerning carbonates, calcite is

predominant (20–30%) over dolomite in these units. Dolomite shows the highest content in Unit VII reaching up to 17% in the sandier layer (PLN-18). In this unit, the presence of gypsum and halite in low contents (<5%), together with traces of muscovite, paragonite, amphiboles and aragonite is remarkable.

Unit VIII is characterized by a higher content in sand fraction than previous units, whereas phyllosilicates (35%) and quartz (around 10%) decrease in comparison with them. In addition, the increase in dolomite and feldspars (plagioclase > potassium feldspar), both rounding 25% is remarkable. Dolomite is the carbonate predominant at the base of this unit being dominant calcite at the top. Traces of halite are also identified.

The silts and muds of Unit IX show an increase in both phyllosilicates (40–55%) and quartz (10–16%), whereas feldspars decrease sharply (<5%). Calcite (20–28%) predominates over dolomite (<10%), remaining gypsum and halite in low content (<5%).

Comparing with the previous unit, Unit X displays a slight decrease in the phyllosilicate content (33–42%), quartz persists in similar abundance (15%) and feldspars (<10%) increase slightly. Both calcite and dolomite content increase, reaching 28% and 11%, respectively. Within phyllosilicates muscovite (Units VI, VIII and IX) and paragonite (Units VII and X) have been identified. Under SEM examination highlights the chaotic texture observed in samples from unit X (Fig. 5c) with the presence of mica grains both as skeletal (sand) and matrix (silt–clay) fractions (Fig. 5d).

Under microscope examination the heavy mineral assemblage is represented by rutile, garnet, chlorite and hornblende with subordinated epidote, zircon andalusite, kyanite, glaucophane, pyroxene, staurolite and opaques (Fig. 7b, c, e, f). The presence of metamorphic rock fragment grains has been also recognized in these units.

**3.1.3.3. Clay mineralogy.** Illite is the main clay mineral (>45%; mean 50%) in Units VII and IX (Fig. 4), with subordinated smectite (26–32%; mean 30%) and kaolinite (19–21%; mean 20%). Traces of random mixed layers (mostly 10–14 Å) have been identified.

Illite displays 002/001 ratios between 0.42 and 0.51 (mean 0.48), the highest of all the samples studied in core PLN. This fact is interpreted as illite enrichment in Al with respect to Mg and Fe in octahedral sheets. The illite crystallinity (FWHM) fluctuates between 0.51 and 0.69 ( $2\theta$ ) with a crystallite size ranging from 13 to 17 nm. In reference to smectites, only the basal sample of Unit VII presents a moderate Biscaye index value (0.33), whereas the remain samples show lower values (0.13 to 0.22) increasing upward.

Clay mineral assemblage is similar to that reported in MFA and UFA, but in this case illite is predominant, showing higher Al/Fe + Mg ratio and lower crystallinity (ordering).

**3.1.3.4. Geochemistry.** Chemically  $\text{Al}_2\text{O}_3$ ,  $\text{Fe}_2\text{O}_3$ ,  $\text{K}_2\text{O}$  and  $\text{TiO}_2$  show a similar trend evolution in Units VI and VII, highlighting only two small peaks in the clayey silts situated near the lower and upper limits of Unit VII, respectively. All these elements increase within the silty sands of Unit VIII, especially  $\text{TiO}_2$  (Fig. 6).

Remarkable changes have been observed in the behaviour of numerous elements in Units IX and X. So although  $\text{Al}_2\text{O}_3$ ,  $\text{K}_2\text{O}$  and  $\text{Fe}_2\text{O}_3$  increase first noteworthy (especially the two last) in Unit IX, a decrease is observed (mainly  $\text{Fe}_2\text{O}_3$ ) in the silty sands of Unit X. Concerning the  $\text{TiO}_2$  abundance, the most remarkable is the increase displayed when passing from Unit IX to X.

The content of  $\text{SiO}_2$  shows no high variations, instead a slight increase in sandy silts and silty sands from Unit VIII and X, respectively.

The abundance of CaO does not show significant variations with a slight increase in Unit X. A slight increase of  $\text{TiO}_2$  was detected in Unit VIII, whereas MgO displays a slight impoverishment from Unit VI to X. On the contrary, the  $\text{Na}_2\text{O}$  abundance increasing upward reaching the highest content in Unit X. Likewise, MnO content is no relevant, although this oxide increase together with  $\text{Al}_2\text{O}_3$ ,  $\text{Na}_2\text{O}$ ,  $\text{K}_2\text{O}$ ,  $\text{Fe}_2\text{O}_3$  and  $\text{TiO}_2$  in sample PLN-21 (Unit VII).

Units IX and X show lower  $\text{P}_2\text{O}_5$  contents than Unit VII, whereas this oxide presents a significant decrease in Unit VIII.

### 3.2. Isotopic composition and vertical variation

Concerning carbonates, is important to have in mind the difficulties to obtain representative non-detrital carbonate samples, even when sampling has been done to avoid bioclasts.

The cross-plot diagram of calcite exhibits a narrow range for  $\delta^{18}\text{O}$  but a spread of values for  $\delta^{13}\text{C}$  (Fig. 8). Thus,  $\delta^{18}\text{O}$  varies between  $-3.97\text{‰}$  and  $-2.90\text{‰}$  (mean  $3.45\text{‰}$ ), whereas  $\delta^{13}\text{C}$  ranges from  $-5.79\text{‰}$  to  $-2.41\text{‰}$  (average  $3.51\text{‰}$ ). In fact, the isotopic analysis of samples from Units I and III (LFA) displays the lower values of  $\delta^{13}\text{C}$ , whereas samples from Unit V (MFA) presents the higher contents and the remaining samples (mostly UFA) show intermediate values between them. The isotopic profile (Fig. 9) shows that  $\delta^{18}\text{O}$  is quite

uniformly distributed with the exception of a small excursion at the base of unit V. On the other hand, carbon from Units I and III ( $\delta^{13}\text{C} = -5.79\text{‰}$  to  $-4.38\text{‰}$ ) is clearly lighter than carbon from Units V to X ( $\delta^{13}\text{C} = -3.75\text{‰}$  to  $-2.41\text{‰}$ ), with the exception of a strong excursion ( $\delta^{13}\text{C} = -4.30$ ) at the top of Unit V (Fig. 9).

Concerning the isotopic analyses of dolomite these are characterized by a wide range of values (Fig. 8) for both  $\delta^{18}\text{O}$  (from  $-4.45\text{‰}$  to  $-2.02\text{‰}$ ) and  $\delta^{13}\text{C}$  (from  $-2.0\text{‰}$  to  $+0.18\text{‰}$ ). The isotopic profile displays values of  $\delta^{13}\text{C}$  clearly heavier than those observed in calcite (Fig. 9) being noteworthy two excursions at the base of both Units V ( $+0.18\text{‰}$ ) and VII ( $-0.52\text{‰}$ ). A different behaviour is observed for  $\delta^{18}\text{O}$ , with a narrower range of values and two small excursions toward lighter oxygen in Units V and VII. It highlights the different trend at top of the section (Unit X), enriched in  $\delta^{18}\text{O}$  but depleted in  $\delta^{13}\text{C}$ .

### 3.3. Palaeontology

The lower facies association is characterized by the scarcity of fossils, with very rare fragmented valves of bivalves (Fig. 10: *Ostrea edulis*, *Venerupis decussatus*), isolated planktonic foraminifers (*Orbulina universa*) and characeans, or rare spines of echinoderms. The ostracode record of these lower 34 m is concentrated mainly in the sandier bed of Unit III (Fig. 11: 22 species; 6 individuals/g), with similar proportions of both brackish-water (e.g., *Cyprideis torosa*, *Leptocythere tenera*, *Loxococoncha elliptica*) and marine species (e.g., *Urocythereis oblonga*, *Semicytherura sulcata*, *Aurila convexa*). In addition, this level includes very abundant spines of echinoderms and frequent specimens of planktonic foraminifers (*Orbulina*, *Globigerina*).

In the middle facies association, the macrofaunal remains (*Glycymeris glycymeris*, *V. decussatus*) are very scarce and fragmented in Unit IV. Microfauna is clearly dominated by brackish assemblages of both ostracodes (*Cyprideis torosa*) and foraminifers (*Ammonia tepida*). In the upper part, fragments of limonitized, reddish to brownish roots are frequent. Remains of carbonized root fragments are very abundant in the basal part of Unit V ( $-54$  to  $-49$  m). Both macrofauna and microfauna present rare individuals of marine species in this interval, with scarce planktonic foraminifers and fragmented specimens of *Quinqueloculina*. These marine forms disappear toward the upper part of this unit, where the fossil record is absent or is composed of either freshwater gastropods or brackish ostracodes ( $<2$  individuals/g).

The above mentioned scarcity contrasts with the abundant fossil record of Unit VI, with very frequent fragments of both infralittoral and epifaunal bivalve assemblages and marine gastropods. The ostracode record (Fig. 11: 10–15 individuals/g) is dominated by *Cyprideis torosa* (30–35%), although this unit contains similar percentages of both brackish and marine forms. Miliolids, rotaliids (*Ammonia beccarii*), planktonic foraminifers, fragments of bryozoans and spines of echinoderms are well represented, together with numerous central diatoms.

The mollusc diversity and abundance of Unit VII decrease toward the top, with numerous fragments of bivalves (mainly *Ostrea edulis* and pectinids) and rare specimens of marine (*Hinia*, and *Rissoa*) and brackish (*Truncatella*) gastropods near the base. Ostracode densities (1–10 individuals/g) decrease toward the top, with the predominance of *Palmoconcha turbida* and the high brackish ostracode assemblage. Fragments of bryozoans, miliolids, rotaliids (*Ammonia beccarii*), planktonic foraminifers (*Globigerina*, *Orbulina*, and *Globigerinoides*), and triaxone spicules of sponges and spines of echinoderms are very abundant, together with numerous carbonaceous remains of roots or plants.

Unit VIII presents a macrofaunal content dominated by fragments of *Venerupis decussatus*, especially abundant in the lower silty sands. This basal layer contains isolated valves of *Cyprideis torosa* and *Palmoconcha turbida*. This unit finishes with an important increase of the ostracode density (9 individuals/g) and diversity (17 species), with numerous valves of *Palmoconcha turbida* (~60%) and the brackish

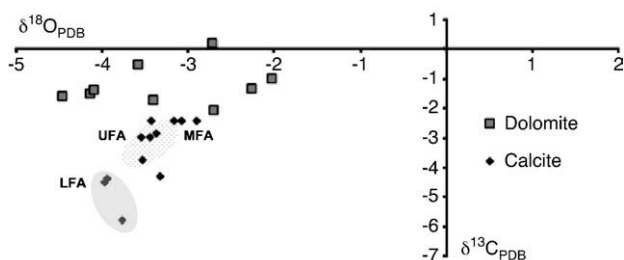


Fig. 8. Isotopic results.  $\delta^{18}\text{O}$  and  $\delta^{13}\text{C}$  cross-plot diagram of carbonates from selected fine-grained sediments.

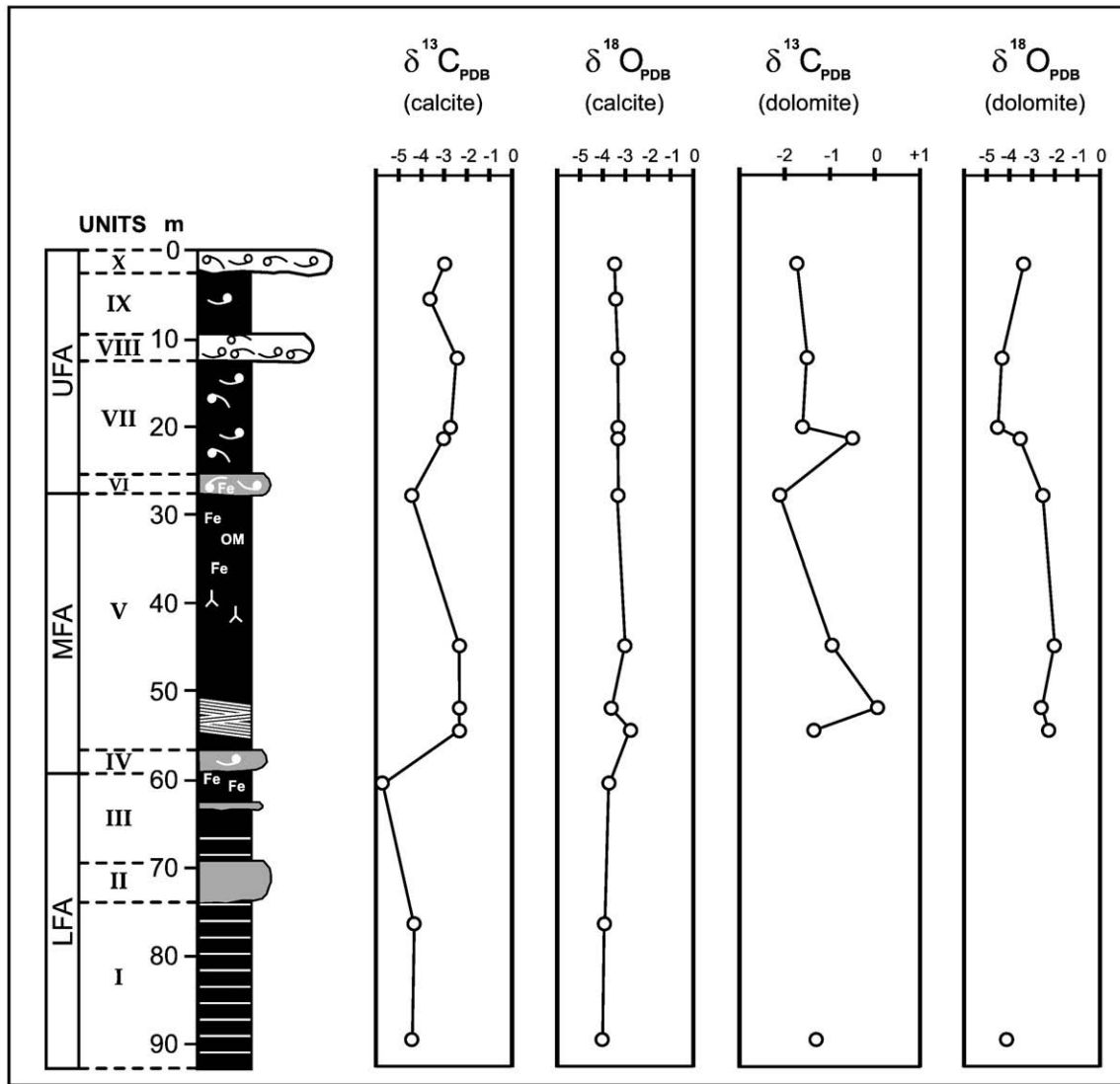


Fig. 9. Vertical isotopic evolution of the core. The position of samples belonging to different facies associations is also indicated.

ostracode assemblage (~20%). Spines of echinoderms and fragments of bryozoans are also very common.

The lower part of Unit IX shows a fossil record similar to Unit VII. Nevertheless, the upper part (–5 to –1.8 m) are characterized by the absence of macrofaunal remains, frequent to very abundant spines of echinoderms and high densities (21–71 individuals/g) of brackish ostracodes that decrease near the top. In these last meters, *Cyprideis torosa* is progressively replaced by *Leptocythere castanea* and *Leptocythere tenera*.

Unit X is characterized by the presence of frequent fragments of *Venerupis decussatus* and rare gastropods near the base. The scarce ostracode faunas (1–2 individual/g) are dominated by *Cyprideis torosa* and *Pontocythere elongata*. Other microfaunal components (miliolids, planktonic foraminifers – *Orbulina universa*, *Globigerina bulloides*, and spines of echinoderms) are more abundant in the uppermost meter of the core.

### 3.4. Radiometric datings

The four radiometric data obtained on bivalve shell indicate an age comprised between 44–42.5 kyr BP (basal part of Unit V; –55.3 m depth) and 3.5–3.2 cal kyr BP (lower part of Unit X). Consequently, an Upper Pleistocene age must be assigned to the lower facies

association, whereas the middle facies association was deposited between the Upper Pleistocene and the Flandrian transgressive maximum (7–6.5 cal kyr BP; Zazo et al., 1994), represented by the marine deposits of Unit VI. The upper four units were deposited during the 6.7–3.0 cal kyr interval (Table 1).

## 4. Discussion

### 4.1. Mineralogical considerations

The main mineralogical features of the three facies associations are shown in Table 2.

Units I and II of LFA are characterized by the relative low content in carbonates but the predominance of siliciclastic minerals (e.g. phyllosilicates, quartz, feldspars), indicating a strong influence of detrital input from the continent. Unit III exhibits similar mineralogical features with the exception of the dolomite-rich (20%) sandy-silt insert. The sediments of MFA still show evidence of detrital input especially in relative coarse-grained facies (base of association), but increasing calcite content in fine-grained lithofacies with a mean value of 28% suggesting, despite the bioclastic content, physico-chemical conditions for carbonate formation in an environment where gypsum precipitation can take also place.



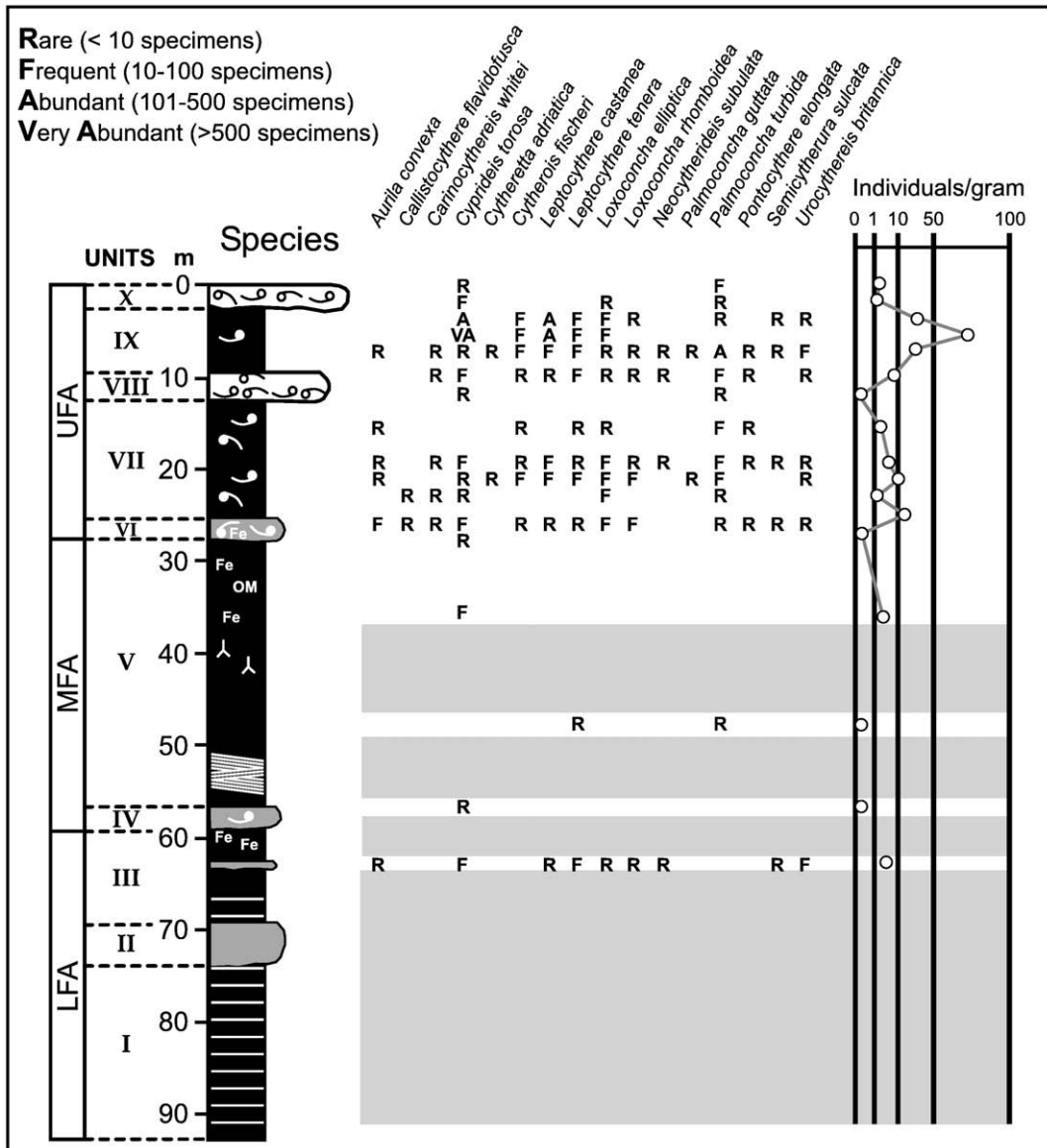


Fig. 11. Ostracode distribution along the PLN core.

provenance source, probably more related to marine sediments input than continental supply.

The heavy minerals distribution and its composition indicate a continuous detrital input from the continent and a mainly igneous-metamorphic parent rock source. The noteworthy increase in rutile and the presence of glaucophane and epidote in the Phase III suggests a possible alternative sedimentary source. The heavy mineral assemblages are similar to those reported in the near Gulf of Cadiz by Gutierrez-Más et al. (1994), where these authors emphasized the role played by sea-level changes, fluvial supplies and/or oceanographic factors in their distribution. The existence of several sources for heavy minerals input may explain the mixing of very stable (e.g. rutile, zircon) and unstable (e.g. garnet, hornblende, epidote) heavy minerals in the studied samples.

Summarizing, from a mineralogenetic point of view: quartz, feldspars, dolomite, heavy minerals, muscovite, paragonite and clay sized phyllosilicates (illite, kaolinite, chlorite, smectite and mixed layers) are considered inherited minerals. Concerning smectite a locally possible neoformation in restricted environment where it can achieve higher structural ordering is not discarded. Among minerals formed by means of precipitation calcite, halite and gypsum are

included. Calcite is also forming bioclastic shells, relatively abundant in some samples.

Results from geochemical analysis are consistent with the mineralogical data as a whole. The behaviour and content of TiO<sub>2</sub> along the borehole is highlighted, with a peak in Unit III associated to dolomite anomaly and two more increases in Units VIII and X associated to relatively coarser grained lithofacies (bioclastic silty sands).

#### 4.2. Palaeoenvironmental reconstruction of the core

Three main phases may be recognized in the palaeoenvironmental sequence of this core (Fig. 12).

##### 4.2.1. Phase 1 (>44 kyr BP)

Units I to III show the most depleted values of δ<sup>13</sup>C and δ<sup>18</sup>O of the studied samples, suggesting inflow of fresh waters, whereas the enrichment in heavy oxygen toward the top indicates a relative increase in evaporation and relatively arid conditions. Lamination and local bioturbation in fine-grained facies suggests a quiet and shallow environment where the mainly grey shades of sediments indicate

**Table 2**  
Summary of mineralogical data. Facies, heavy minerals and bulk and clay mineralogy are included. P: Phyllosilicates; Q: Quartz; F: Feldspars; C: Calcite; D: Dolomite; G: Gypsum; H: Halite; A: Aragonite.

Facies association	Bulk mineralogy (mean values %)	Heavy minerals	Clay minerals (mean values %)	Biscaye index (smectite)	FWHM (illite)	Al/Mg + Fe (illite)
Upper (UFA) Units VI, VII, VIII, IX, X	(VIII, X) Silty sands: P <sub>36</sub> Q <sub>12</sub> F <sub>13</sub> C <sub>23</sub> D <sub>13</sub> H <sub>&lt;5</sub> (VII, IX) Silts: P <sub>47</sub> Q <sub>15</sub> F <sub>6</sub> C <sub>23</sub> D <sub>6</sub> G <sub>&lt;5</sub> H <sub>&lt;5</sub> (VI, VII) Sandy silts: P <sub>37</sub> Q <sub>16</sub> F <sub>5</sub> C <sub>30</sub> D <sub>11</sub> H <sub>&lt;5</sub> A <sub>&lt;1</sub> (P = muscovite, chlorite, paragonite, clay minerals)	Rutile–garnet–chlorite–hornblende > epidote–zircon–andalusite–kyanite–glaucofane–staurolite–pyroxene–opaques	Smectite (30) Illite (50) Kaolinite (20) (traces of random mixed layers)	0.13–0.33	0.51–0.69	0.42–0.51 (0.48)
Middle (MFA) Units IV, V	(V) Muds: P <sub>50</sub> Q <sub>9</sub> F <sub>5</sub> C <sub>29</sub> D <sub>7</sub> (V) Silts: P <sub>29</sub> Q <sub>15</sub> F <sub>10</sub> C <sub>28</sub> D <sub>17</sub> G <sub>&lt;5</sub> (IV) Silty sands: P <sub>24</sub> Q <sub>34</sub> F <sub>23</sub> C <sub>8</sub> D <sub>11</sub> (P = muscovite, chlorite, paragonite, clay minerals)	Garnet–rutile–titanite–zircon–hornblende > kyanite–andalusite–opaques–hematite–chlorite	Smectite (47) Illite (37) Kaolinite (16) (traces of random mixed layers)	0.14–0.31	0.38–0.55	0.26–0.31 (0.29)
Lower (LFA) Units I, II, III	(II) Silty sands: P <sub>28</sub> Q <sub>39</sub> F <sub>13</sub> C <sub>15</sub> D <sub>5</sub> (I, III) Silts and muds: P <sub>51</sub> Q <sub>12</sub> F <sub>10</sub> C <sub>20</sub> D <sub>7</sub> (P = micas, clay minerals)	Garnet–rutile > hornblende–pyroxene–staurolite–opaques	Smectite (40) Illite (42) Kaolinite (18) (traces of random mixed layers)	<0.2	0.31–0.54	0.38–0.51 (0.43)

reducing conditions, supporting the evidence of organic activity the P<sub>2</sub>O<sub>5</sub> content in bioturbated grey silts. At top of Unit III redox changes occur as evidenced by reddish stains (iron oxides) coating planes suggesting subaerial exposure of sediments. The mineralogical results corroborate a depositional environment where clay/silt decantation (phyllosilicates mainly) and calcite precipitation take place, originating fine-grained facies. These data agree with the pollen results of

Zazo et al. (1999), which inferred the presence of freshwater marshes in the Doñana National Park during the Upper Pleistocene.

The insert of sandy coarse-grained facies (Unit II) indicates detrital input from fluvial origin, consisting mainly of quartz and feldspars. Chemical analysis corroborates that SiO<sub>2</sub> increase noteworthy in the silica-rich detrital input besides Na<sub>2</sub>O and K<sub>2</sub>O (feldspars and micas) but depleted in Fe<sub>2</sub>O<sub>3</sub>, TiO<sub>2</sub> and MnO.

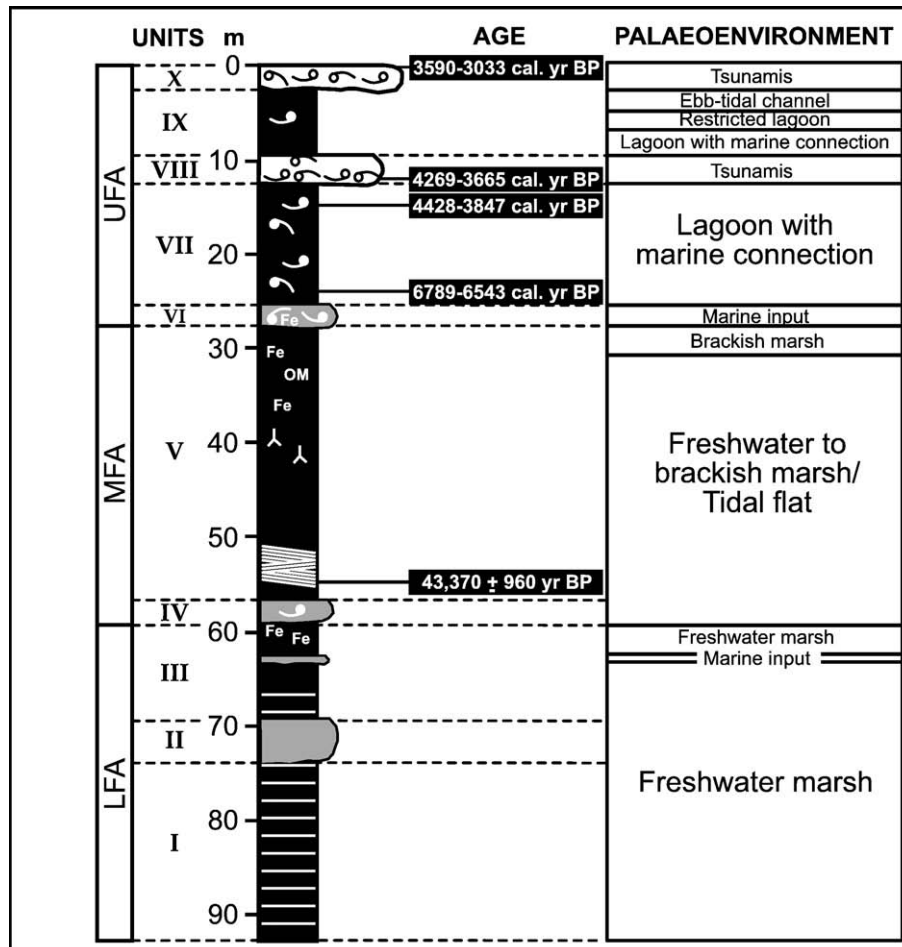


**Fig. 12.** Palaeoenvironmental reconstruction of the core PLN. The sedimentary environment and dating are shown.

The thin sandy insert in Unit III shows significant compositional and palaeontological features indicating a change in palaeoenvironmental conditions. So, the high content in dolomite besides the increase of MgO, Fe<sub>2</sub>O<sub>3</sub> (justifying the ochre color of sediment), MnO and TiO<sub>2</sub> is noteworthy. Regarding this level a proximity to a brackish lagoon may be inferred by the presence of frequent high brackish-water ostracode species (*Cyprideis torosa*, *Leptocythere* spp., and *Loxiconcha elliptica*). These species are very common in perimediterranean, shallow brackish lagoons with salinities up to 25‰ in most cases (Marocco et al., 1996; Ruiz et al., 2000a; Ruiz et al., 2006a). The occurrence of some infralittoral species (*Aurila convexa*, *Semicytherura sulcata*, and *Urocythereis britannica*), very abundant in the adjacent marine environments of the Cádiz Gulf (Ruiz et al., 1997), will be indicative of a tidal, marine connection of this lagoon. This level will represent a temporal inundation of this area and has been also observed in a long core drilled near the Lucio Mari López (see Fig. 1; Zazo et al., 1999).

#### 4.2.2. Phase 2 (44–7 cal kyr BP)

The relatively high content of quartz and feldspars at the base of the MFA, besides the existence of sedimentary structures (lamination) and increasing sand–silt grains, indicates persistence of detrital input. The remarkable increase of calcite in sediments with phyllosilicates predominant (Unit V), account for physico-chemical conditions favouring the precipitation of carbonates. In the upper part of unit V the muds containing organic matter and carbonaceous plant debris indicate reducing stagnant environment with high biological productivity. Moreover the existence at top of reddish-ochre stains and nodules of limonite suggests an oscillating water level. On the other hand the first occurrences of gypsum in this unit indicate evaporites formation probably from evaporation of marine water input.

Chemical analysis of major elements is coherent with mineralogy displaying slight variations of Al<sub>2</sub>O<sub>3</sub>, SiO<sub>2</sub>, Na<sub>2</sub>O, and TiO<sub>2</sub>. MgO and Fe<sub>2</sub>O<sub>3</sub> contents show higher variability, in the case of iron due to stains and nodules of limonite in organic matter-bearing clayey sediments. The increase of MnO at top of the unit support oxidizing conditions and the P<sub>2</sub>O<sub>5</sub> variations are related to biological activity (bioturbated levels).

Faunal record of Units IV and V is characterized by the alternation of either almost sterile layers or fine beds with the presence of very scarce specimens of either brackish or freshwater species. Some of these layers present evidences of oxidation and show frequent carbonization of phanerogam remains. These variations may be assimilated to a variable, peripheral environment (tidal flat, salt marsh, and fresh marsh) within a lagoon complex, with periodical tidal inundation or freshwater inputs. This variability is contrasted by the changing  $\delta^{13}\text{C}$  record, suggesting a mixing of chemically different waters, and the presence of two layers (–52 to –48 m; –33 to –27.5 m) with marine faunas (miliolids, planktonic foraminifera, and spines of echinoderms) and frequent individuals of brackish ostracode species. These features may be indicative of a temporal transition to intertidal conditions.

#### 4.2.3. Phase 3 (7–3 cal kyr BP)

The units consisting of relative coarse-grained facies (VIII, X and the sandy insert in Unit VII) are interpreted as a detrital input highlighting the increase of feldspar and dolomite contents, whereas a decrease in phyllosilicate abundance. The noteworthy increase of TiO<sub>2</sub> in sandy units (VIII and X) is the most relevant geochemical feature. The existence of laminated and locally bioturbated mud sediments inserted between coarse-grained facies involve quiet stages where mainly settling sedimentation takes place. The occurrences of gypsum and halite support seawater influence and evaporative conditions.

Unit VI presents a diversified and abundant fauna dominated by brackish and marine species. This unit can be interpreted as a new period of inundation, with the introduction of numerous valves of both bivalves and ostracodes during the tidal fluxes.

Unit VII and the basal part of Unit IX contain a microfaunal record very similar to that observed in the sandier level of Unit III, although they differ in the higher abundance of marine bivalves, bryozoans and planktonic foraminifera. Consequently, these units will have settled in a lagoon with a more open marine connection than the lower level. This marine influence is also inferred from the isotopic data, with a relative enrichment of  $\delta^{13}\text{C}$  whereas  $\delta^{18}\text{O}$  remains almost invariable.

In the middle part of Unit IX, the higher number of ostracode specimens (mainly *Cyprideis torosa* and *Loxiconcha elliptica*) and the disappearance of the marine macrofauna can be interpreted as a restriction of the tidal fluxes. These vertical changes indicate an evolution toward a more restricted lagoon and have been observed in other perimediterranean lagoons (Carbonel, 1980; Ruiz et al., 2006b). This regressive trend is confirmed by the progressive replacement of these species by small leptocytherids in the upper part of Unit IX, which characterizes the transition toward the quieter, ebb-tide channels that drain the adjacent salt marshes in the southwestern Spanish estuaries (Ruiz et al., 2000b).

The basal levels of Units VIII and X are disposed unconformably over the lagoon deposits and are characterized by: a) coarser sediments, with up to 35% of medium and fine sands; b) a remarkable bimodal grain-size distribution (see Fig. 3); c) a decrease in sorting; d) a diminution of phyllosilicates, associated to increasing percentages of feldspars; e) an increasing dolomite content; f) a remarkable decrease in illite crystallinity; g) a sudden introduction of marine bivalves and microfauna; and h) a strong decrease or the almost disappearance of the brackish ostracode assemblage. These features can be interpreted as consequences of high-energy, marine events and some of them have been observed in Holocene tsunamigenic deposits of the southwestern Spanish coasts (Lario et al., 2000; Luque et al., 2001; Luque, 2002; Ruiz et al., 2004, 2005a).

### 4.3. Isotopic data and water parameters

Despite the small number of samples analyzed the general trends of calcite isotopic data permits to deduce some interesting changes in the physical–chemical parameters of waters. Concerning dolomite the wide range of values for both  $\delta^{18}\text{O}$  and  $\delta^{13}\text{C}$  seems to be related to its inherited origin and therefore is not discussed below.

In a general perspective, the uniformity of  $\delta^{18}\text{O}$  values through the core PLN contrasts with the distinct sedimentological features of the units differentiated. A relatively rapid throughflow in the water body and/or a deposition of the studied deposits close to inflow points of freshwaters into the basin could account for the recorded persistent low to moderate salinity conditions in spite of low and high stand periods up to subaerial exposure of the area as shown by both sedimentological and palaeontological data. According to some authors (Gofiantini, 1986; Talbot, 1990), small variations in the oxygen isotopes of carbonate from lakes reflect moderate changes in the water temperature and salinity, and in the hydrological balance (inflow–evaporation) between the periods of carbonate precipitation. Consequently, the small variations observed of  $\delta^{18}\text{O}$  values suggest minor effects by evaporation on the isotopic composition of the carbonates, which were formed probably under continuous freshwater inflows.

In contrast to the  $\delta^{18}\text{O}$  values, the  $\delta^{13}\text{C}$  ones vary from bottom to top of the core, with significant progressive drops in Unit III, top of Unit V and Unit IX. Likewise is remarkable the relative shift toward heavier values in Units V, VII, VIII and X. The  $\delta^{13}\text{C}$  enrichment may reflect a photosynthetic fractionation effect enhanced by high biological productivity (Deines, 1980) or a water reequilibration with the atmospheric reservoir (Hoefs, 1987). In contrast, the decomposition of organic matter at lagoon bottom or in sediment porewater may explain the incorporation of isotopically light bicarbonate (<sup>12</sup>C-enriched).

The negative values of  $\delta^{13}\text{C}$  in Units I and III suggest incorporation of organic-derived <sup>13</sup>C-depleted carbon. The carbon isotopic ratio of the dissolved bicarbonate in the lagoon water, and consequently that

of primary carbonates, is affected by the contribution of soil-derived CO<sub>2</sub>. Therefore the light δ<sup>13</sup>C signatures of these units could reflect both the influx of terrestrial carbon and/or the contribution of CO<sub>2</sub> from degraded organic matter related to benthic plants. The more negative δ<sup>13</sup>C values of carbonates in Unit III likely reflect prolonged interaction with isotopically light CO<sub>2</sub>.

The high δ<sup>13</sup>C content detected in the base of Units V and VII may reflect either isotopic reequilibration of the dissolved HCO<sub>3</sub><sup>-</sup> with the atmospheric reservoir (Hoefs, 1987), or contribution of algae and cyanobacteria that may also contribute favouring more enriched carbon isotope compositions in the coastal-marine environment.

The absence of a link between oxygen and carbon isotopes in Unit VII, probably reflects a marked instability in the hydrology of the system, extending upwards. In fact, a drop in δ<sup>13</sup>C of about -1.33‰ in the transition (Unit IX) between the two high-energy events recognized (Units VIII and X) is noteworthy.

In addition, the analysis of the δ<sup>18</sup>O–δ<sup>13</sup>C covariance provides some interesting insights for the interpretation of the isotopic signatures of the core PLN samples in terms of palaeohydrological implications. A clear covariance between δ<sup>18</sup>O and δ<sup>13</sup>C values is characteristic of carbonates formed in total or partially closed environments while carbonates from hydrologically open environments show little or no correlation between oxygen and carbon variations (Talbot, 1990). The calcite samples analyzed from core PLN display a moderate correlation (Fig. 8: R<sup>2</sup>=0.55). In fact, carbonates from core PLN were probably deposited in a marginal lagoon area influenced by continuous freshwater inflow and local seawater input. Under these circumstances, lagoon waters were more or less permanently renewed, so that the geochemical signature of the carbonate deposits matches that of short-residence-time open lakes.

In summary, calcite from the core studied display isotopic compositions indicative of precipitation from isotopically poorly evolved waters as a result of their proximity to the entering of fresh waters. The carbonates therefore show, especially in the upper units, an isotopic behaviour similar to that expected for open lagoon waters.

#### 4.4. Late Pleistocene–Late Holocene palaeoenvironmental evolution of the southwestern Doñana National Park

The lower 60 m of the core includes probably the sedimentological record of the last cold stage (MIS 4 to MIS 2) in this area. The Doñana National Park was a very changing environment during these isotopic stages, with local variations from freshwater to salt marsh and even intertidal conditions. The pollen record of core ML studied by Yll et al. (2003) indicates the passage from the xeric conditions of MIS 4 (*Pinus* and *Artemisia*) to an increasing hydric availability (Poeaceae and Cyperaceae) at the beginning of the MIS 3.

During these stages, this zone was inundated temporarily by marine inputs (sandy layer of Unit III and basal part of Unit V). These layers may be related tentatively to: a) short-lived warmer episodes of interstadial character (Glinde: 51–48 kyr BP; Moershoofd: 46–44 kyr BP) indicated by Behre (1989) in northern and western Europe; b) ice retreat phases deduced by Duplessy et al. (1988) between 55 and 45 kyr; c) the final phase of a warm period in France and Italy (Van Andel, 2003); d) a sea-level rise inferred from emergent coral terraces in Papua New Guinea at cal. 45–43 kyr BP (Yokoyama et al., 2001); or e) high-energy events.

In addition, the palaeocoastline position changed remarkably in connection with the main sea-level changes inferred during this interval. It was situated at 30–35 km seaward at 15 kyr BP (sea level ~-110 m) and more close to the present-day location at 10–12 kyr BP (sea level ~-70 to -50 m), according to several investigations based on high-resolution seismic profiles of the Cádiz Gulf and additional coastal studies (see review in Lobo et al., 2001).

During the Early Holocene (upper part of Unit V), the transition from supratidal/freshwater environments to intertidal, lagoon condi-

tions suggest a progressive sea-level rise. This evolution has been also observed in the adjacent Guadalete estuary, with an increase of the marine inputs between 8 and 7 kyr BP (Goy et al., 1996). In this interval, global sea level rose from a position at around -50 ± 6 m at 10 kyr BP to -5 ± 5 m at 7 kyr BP in this area (Hernández-Molina et al., 1994; Lario, 1996).

The age of Unit VI coincides with the maximum of the Flandrian transgression in this area (~6500 cal years BP; Zazo et al., 1994). At this time, the southwestern Spanish fluvial valleys were inundated and marine sediments of this age have been found in the near Tinto–Odiel estuary (Borrego et al., 1999).

The palaeoenvironmental interpretation of Units VII and IX (~4300–3000 cal years BP) includes the evolution of an open lagoon with a progressive restriction of the sea inputs. Both archaeological data and palaeogeographical reconstructions confirm the presence of a broad lagoon in this area between 1250 and 750 BC (Gómez Toscano, 2006). In addition, the first historical descriptions of this littoral, made by the chronicler Strabo (7–29 BC) and Mela (forty years later), referred to the southern part of the Guadalquivir estuary as an inland lagoon called *Lacus Ligustinus* (García Bellido, 1947).

This evolution is interrupted by two tsunamis that deposited the basal, bioclastic layers of Units VIII (4200–3600 cal years BP) and X (3600–3000 cal years BP). These bioclastic sediments present similar features and ages to other tsunamigenic deposits of this area (Ruiz et al., 2005b; Rodríguez Vidal et al., 2009). In addition, a similar age (3550 ± 35 years BP) has been obtained for a high-energy event that deposited a debris flow in deep cores collected near Portugal (Vizcaino et al., 2006).

## 5. Conclusions

A general scenario for Late Pleistocene–Late Holocene evolution of the Doñana National Park has been proposed, based on the multidisciplinary analysis (lithofacies, texture, bulk and clay mineralogy, isotopes, palaeontology, and dating) of sediments present in a long drill core.

From a compositional point of view the inherited assemblages including phyllosilicates, quartz, feldspars, heavy minerals and dolomite are predominant. Minerals originated by chemical precipitation include calcite, gypsum and halite. The clay mineral assemblage consists of illite, smectite and kaolinite with traces of randomly mixed layers. Changes in the ordering of illite and smectite besides crystallochemical differences (Al/Fe + Mg) in octahedral sheet of illites are the most relevant features. Geochemically the increase of TiO<sub>2</sub> abundance related to sediments with palaeontological evidence of marine input is remarkable. The isotopic composition of calcite and its behaviour is consistent with that expected for open lagoon waters influenced by a continuous freshwater inflow and local seawater input.

The overall study permits to delimitate three main phases since the Late Pleistocene, with an evolution from freshwater marshes to a restricted brackish lagoon. Fresh to brackish marshes (>10 kyr BP) were characterized by clayey-silty, phyllosilicate-rich deposits with depleted isotopic ratios and a remarkable scarcity of both macrofauna and microfauna. These marshes were inundated by a marine input at ~47 kyr BP, being replaced by brackish marshes between ~10 and 7 kyr BP. These marshes were inundated temporary during the maximum of the Flandrian transgression (~6500 cal years BP), with introduction of both marine sediments and faunas. The final phase (6500–3000 cal years BP) is characterized initially by the presence of an open lagoon, with a progressive infilling, the consequent restriction of the tidal fluxes and the apparition of ebb-tide assemblages.

This evolution includes several tsunamigenic layers between 4200 and 3000 cal years BP. These high-energy events are characterized by bimodal grain-size distribution, sorting decrease, crystallochemical

changes in illites, increasing dolomite content and TiO<sub>2</sub> anomaly. The main geological features and datings of these beds coincide with those deduced for other tsunamigenic deposits of southern Iberia and permit to contrast the evidence of periodic high-energy events during the Holocene in this area.

## Acknowledgements

This work was funded by two Spanish DGYCIT Projects (CTM2006-06722 and CGL2006-01412) and three Research Groups of the Andalusia Board (RNM-238, RNM-293 and RNM-349).

## References

- Anderson, T.F., Arthur, M., 1983. Stable isotopes of oxygen and carbon and their application to sedimentologic and paleoenvironmental problems. *Soc. Econ. Paleontol. Mineral. Short Course* 10, 1–151.
- Bao, R., Alonso, A., Delgado, C., Pagés, J.L., 2007. Identification of the main driving mechanisms in the evolution of a small coastal wetland (Traba, Galicia, NW Spain). *Paleogeog., Palaeoclimatol., Palaeoecol.* 247, 296–312.
- Barahona, E., 1974. Arcillas de ladrillería de la provincia de Granada: evaluación de algunos ensayos de materias primas. Ph.D. Thesis, Granada University, Granada.
- Behre, K.E., 1989. Biostratigraphy of the last glacial period in Europe. *Quat. Sci. Rev.* 8, 25–44.
- Borrego, J., Ruiz, F., González-Regalado, M.L., Pendón, J.G., Morales, J.A., 1999. The Holocene transgression into the estuarine central basin of the Odiel River mouth (Cádiz Gulf, SW Spain): lithological and faunal assemblages. *Quat. Sci. Rev.* 18, 769–788.
- Canali, G., Capraro, L., Donnia, S., Rizzetto, F., Serandrei-Barbero, R., Tosi, L., 2007. Vegetational and environmental changes in the eastern Venetian coastal plain (Northern Italy) over the past 80,000 years. *Paleogeog., Palaeoclimatol., Palaeoecol.* 253, 300–316.
- Carbonel, P., 1980. Les ostracodes et leur intérêt dans la définition des écosystèmes estuariens et de plateforme continentale. *Essais d'application à des domaines anciens. Mém. Inst. Géol. Bass. d'Aquitaine* 11, 1–350.
- Carretero, M.I., Ruiz, F., Rodríguez Ramírez, A., Cáceres, L., Rodríguez Vidal, J., González-Regalado, M.L., 2002. The use of clay minerals and microfossils in palaeoenvironmental reconstructions: the Holocene littoral strand of Las Nuevas (Doñana National Park, SW Spain). *Clay Minerals* 37, 93–103.
- Chamley, H., 1989. *Clay Sedimentology*. Springer Verlag, Berlin. 623 pp.
- Cearreta, A., Cachao, M., Cabral, M.C., Bao, R., Ármalo, M.J., 2003. Lateglacial and Holocene environmental changes in Portuguese coastal lagoons 2: microfossil multiproxy reconstruction of the Santo André coastal area. *The Holocene* 13, 447–458.
- Clague, J.J., Bobrowsky, P.T., Hutchinson, I., 2000. A review of geological records of large tsunamis at Vancouver Island, British Columbia. *Quat. Sci. Rev.* 19, 849–863.
- Compton, J.H., 2007. Holocene evolution of the Anichab Pab on the south-west coast of Namibia. *Sedimentology* 54, 55–70.
- Craig, H., 1957. Isotopic standards for carbon and oxygen correction factors for mass spectrometric analysis of carbon dioxide. *Geochim. Cosmochim. Acta* 12, 133–149.
- De la Vega, A.C., Keen, D.H., Jones, R.L., Wells, J.M., Smith, D.E., 2000. Mid-Holocene environmental changes in the Bay of Skail, Mainland Orkney, Scotland: an integrated geomorphological, sedimentological and stratigraphical study. *J. Quat. Sci.* 15, 509–528.
- Deines, P., 1980. The isotopic composition of reduced organic carbon. *Handbook of Environmental Isotope Geochemistry 1. The Terrestrial Environment*, A. Elsevier Sc. Publ. Amsterdam, pp. 329–406.
- Duplessy, J.C., Shackleton, N.J., Fairbanks, R.G., Labeyrie, L., Oppo, D., Kallel, N., 1988. Deepwater source variations during the last climatic cycle and their impact on the global deep circulation. *Palaeoceanography* 3, 343–360.
- Edwards, R.J., 2001. Mid-to late Holocene relative sea-level change in Poole Harbour, southern England. *J. Quat. Sci.* 16, 221–235.
- Esquevin, J., 1969. Influence de la composition chimique des illites sur la cristallinité. *Bull. Centre. Rech. Pau. S.N.P.A.* 3, 147–154.
- Folk, R.L., 1980. *Petrology of Sedimentary Rocks*. Hemphill Publishing Co, Austin Texas. 182 p.
- Fontana, S., 2005. Holocene vegetation history and palaeoenvironmental conditions on the temperate Atlantic coast of Argentina, as inferred from multi-proxy lacustrine records. *J. Paleolimnol.* 34, 445–469.
- García Bellido, A., 1947. *La España del siglo primero de nuestra era (según P. Mela y C. Plinio)*. Colección Austral. Ed. Espasa Calpe. 301 p.
- Gerdes, G., Petselberger, B.E.M., Scholz-Bottcher, B.M., Streif, H., 2003. The record of climatic change in the geological archives of shallow marine, coastal, and adjacent lowland areas of Northern Germany. *Quat. Sci. Rev.* 22, 101–124.
- Gofiantini, R., 1986. Environmental isotopes in lake studies. In: Frit, P., Fontes, J.H. (Eds.), *Handbook of Environmental Isotope Geochemistry 2*. Elsevier Sc. Publ. Amsterdam, pp. 113–168.
- Gómez Toscano, F., 2006. El final de la Edad de Bronce entre el Guadiana y el Guadalquivir. Síntesis histórico-arqueológica según las más recientes evidencias. *Sondead. Madrider Mitteil.* 47, 24–42.
- Goy, J.L., Zazo, C., Dabrio, C.J., Lario, J., Borja, F., Sierro, F.J., Flores, J.A., 1996. Global and regional factors controlling changes of coastlines in southern Iberia (Spain) during the Holocene. *Quat. Sci. Rev.* 15, 773–780.
- Grauert, M., Björck, S., Sonderik, S., 2001. Storegga tsunami deposits in a coastal lake on Suduroy, the Faroe Islands. *Boreas* 30, 263–271.
- Gutiérrez-Más, J.M., Domínguez-Bella, S., López-Aguayo, F., 1994. Present-day sedimentation patterns of the Gulf of Cadiz northern shelf from heavy minerals analysis. *Geo-Mar. Lett.* 14, 52–58.
- Kontopoulos, N., Avramidis, P., 2003. A late Holocene record of environmental changes from the Alikí Lagoon, Egeion, North Peloponnese, Greece. *Quat. Int.* 111, 75–90.
- Hayward, B.W., Grenfell, H.R., Sandiford, A., Shane, P.R., Morley, M., Alloway, B.V., 2002. Foraminiferal and molluscan evidence for the Holocene marine history of two breached maar lakes, Auckland, New Zealand. *J. Geol. Geoph.* 45, 467–479.
- Hernández-Molina, F.J., Somoza, L., Rey, J., Pomar, L., 1994. Late Pleistocene–Holocene sediments in the Spanish continental shelves: model for very high-resolution sequence stratigraphy. *Mar. Geol.* 120, 129–174.
- Hoefs, J., 1987. *Stable Isotope Geochemistry*. Springer-Verlag, Berlin. 241 p.
- Lario, J., 1996. Último y Presente Interglacial en el área de conexión Atlántico-Mediterráneo: variaciones del nivel del mar, paleoclima y paleoambientes. Ph. D. Thesis, Universidad Complutense de Madrid, Madrid. 269 pp.
- Lario, J., Zazo, C., Plater, A.J., Goy, J.L., Dabrio, C.J., Borja, F., Sierro, F.J., Luque, L., 2000. Particle size and magnetic properties of Holocene estuarine deposits from the Doñana National Park (SW Iberia): evidence of gradual and abrupt coastal sedimentation. *Zeit. Geomorphol.* 45, 33–54.
- Lobo, F.J., Hernández-Molina, F.J., Somoza, L., Díaz del Río, V., 2001. The sedimentary record of the post-glacial transgression on the Gula of Cadiz continental shelf (Southwest Spain). *Mar. Geol.* 178, 171–195.
- Luque, L., 2002. Cambios en los paleoambientes costeros del sur de la Península Ibérica durante el Holocene. Ph. D. Thesis, C.S.I.C.-Universidad Complutense de Madrid, Madrid. 343 p.
- Luque, L., Lario, J., Zazo, C., Goy, J.L., Dabrio, C.J., Silva, P.G., 2001. Tsunami deposits as palaeoseismic indicators: examples from the Spanish coast. *Acta Geol. Hisp.* 3–4, 197–211.
- Luque, L., Lario, J., Civis, J., Silva, P.G., Zazo, C., Goy, J.L., Dabrio, C.J., 2002. Sedimentary record of a tsunami during Roman times, Bay of Cadiz, Spain. *J. Quat. Sci.* 17, 623–631.
- Marocco, R., Melis, R., Montenegro, M.E., Pugliese, N., Vio, E., Lenardon, G., 1996. Holocene evolution of the Caorle barrier lagoon (northern Adriatic Sea, Italy). *Riv. Ital. Paleontol. Stratigr.* 102, 385–396.
- Mason, G.M., Surdam, R.C., 1992. Carbonate mineral distribution and isotope fractionation: an approach to depositional environment interpretation, Green River Formation, Wyoming, U.S.A. *Chem. Geol.* 101, 311–321.
- McCrea, J.M., 1950. On the isotope geochemistry of carbonates and a paleotemperature scale. *J. Chem. Phys.* 18, 849–857.
- Pozo, M., Carretero, M.I., Ruiz, F., Rodríguez Vidal, J., Cáceres, L.M., Abad, M., 2008. Caracterización mineralógica de facies sedimentarias de edad Pleistoceno superior–Holoceno en el Parque Nacional de Doñana (Huelva). *Implicaciones paleoambientales. Geotemas* 10, 953–956.
- Reeves, J.M., Chivas, A.R., Gracia, A., De Deckker, P., 2007. Palaeoenvironmental changes in the Gulf of Carpentaria (Australia) since the last interglacial based on Ostracoda. *Paleogeog., Palaeoclimatol., Palaeoecol.* 246, 163–187.
- Rodríguez Vidal, J., Ruiz, F., Cáceres, L.M., 2009. Comment on “Formation of chenier plain of the Doñana marshland (SW Spain): Observations and geomorphic model”. *Mar. Geol.* 263, 120–122.
- Ruiz, F., González-Regalado, M.L., Muñoz, J.M., 1997. Multivariate analysis applied to total and living fauna: seasonal ecology of recent benthic ostracoda off the North Cadiz Gulf Coast (SW Spain). *Mar. Micropaleontol.* 31, 183–203.
- Ruiz, F., González-Regalado, M.L., Baceta, J.I., Menegazzo-Vitturi, L., Pistolato, M., Rampazzo, G., Molinaroli, E., 2000a. Los ostrácodos actuales de la laguna de Venecia (NE de Italia). *Geobios* 33, 447–454.
- Ruiz, F., González-Regalado, M.L., Baceta, J.I., Muñoz, J.M., 2000b. Comparative ecological analysis of the ostracod faunas from low- and high-polluted Spanish estuaries: a multivariate approach. *Mar. Micropal.* 40, 345–376.
- Ruiz, F., Rodríguez-Ramírez, A., Cáceres, L.M., Rodríguez Vidal, J., Carretero, M.I., Clemente, L., Muñoz, J.M., Yañez, C., Abad, M., 2004. Late Holocene evolution of the southwestern Doñana National Park (Guadalquivir Estuary, SW Spain): a multivariate approach. *Paleogeog., Palaeoclimatol., Palaeoecol.* 204, 47–64.
- Ruiz, F., Rodríguez-Ramírez, A., Cáceres, L.M., Rodríguez Vidal, J., Carretero, M.I., Abad, M., Ollás, M., Pozo, M., 2005a. Evidence of high-energy events in the geological record: Mid-Holocene evolution of the southwestern Doñana National park (SW Spain). *Paleogeog., Palaeoclimatol., Palaeoecol.* 229, 212–229.
- Ruiz, F., Rodríguez-Ramírez, A., Cáceres, L. M., Rodríguez Vidal, J., Carretero, M. I., Abad, M., Ollás, M., Pozo, M., 2005b. Eventos de alta energía durante el Holoceno Medio y reciente en el Parque Nacional de Doñana (SO de España). VI Reunión de Cuaternario Ibérico. Gibraltar, UK.
- Ruiz, F., Abad, M., Galán, E., González, I., Aguilá, I., Ollás, M., Gómez Ariza, J.L., Cantano, M., 2006a. The present environmental scenario of El Melah Lagoon (NE Tunisia) and its evolution to a future sabkha. *J. African Earth Sci.* 44, 289–302.
- Ruiz, F., Abad, M., Ollás, M., Galán, E., González, I., Aguilá, E., Hamoumi, N., Pulido, I., Cantano, M., 2006b. The present environmental scenario of the Nador Lagoon (Morocco). *Envir. Res.* 102, 215–229.
- Sakamoto, W., 1972. Study of the Process of River Suspension from Flocculation to Accumulation in Estuary, 5. *Bull. Ocean Res. Inst. Tokyo*. 46 p.
- Schultz, L.G., 1964. Quantitative interpretation of mineral composition from X-ray and chemical data for the Pierre Shale. United States Geological Survey, Prof. Paper, p. 391C.

- Singarasubramanian, S.R., Mukesh, M.V., Manoharan, K., Murugan, S., Bakkiaraj, D., Meter, A.J., Seralathan, P., 2006. Sediment characteristics of the M-9 tsunami event between Rameswaram and Thoothukudi, Gulf of Mannar, southeast coast of India. *Sci. Tsunami Hazards* 25, 160–172.
- Skrabal, S.A., 1991. Clay mineral distributions and source discrimination of Upper Quaternary sediments, lower Chesapeake Bay, Virginia. *Estuaries* 14, 29–37.
- Soares, A.M.M., 2008. Radiocarbon dating of marine samples from Gulf of Cadiz. Abstracts Annual Conference IGCP 495, Faro, Portugal, pp. 6–7.
- Stuiver, M., Reimer, P.J., 1993. Radiocarbon calibration program. *Rev. 4.2. Radiocarbon* 35, 215–230.
- Stuiver, M., Reimer, P.J., Bard, E., Beck, J.W., Burr, G.S., Hughen, K.A., Kromer, B., McCormac, F.G., van der Plicht, J., Spurk, M., 1998. INTCAL98 Radiocarbon age calibration 24,000–0 cal BP. *Radiocarbon* 40, 1041–1083.
- Talbot, M.R., 1990. A review of the paleohydrological interpretation of carbon and oxygen isotopic ratios in primary lacustrine carbonates. *Chem. Geology. (Isot. Geosci. Sect.)* 80, 261–279.
- Tripanas, E.K., Bryant, W.R., Slowey, N.C., Bouma, A.H., Karageorgis, A.P., Berti, B., 2007. Sedimentological history of Bryant Canyon area, northwest Gulf of Mexico, during the last 135 kyr (Marine Isotope Stages 1–6): a proxy record to Mississippi River discharge. *Paleogeog., Palaeoclimatol., Palaeoecol.* 246, 137–161.
- Van Andel, T.H., 2003. Glacial environments I – the Weichselian climate in Europe between the end of the OIS – Interglacial and the Last Glacial Maximum. In: Van Andel, T., Davies, W. (Eds.), *Archaeological Results of the Stage 3 Project*. The McDonald Institute for Archaeological Research, Cambridge, pp. 10–20.
- Vizcaino, A., Gràcia, E., Escutia, C., Asioli, A., García-Orellana, J., Lebreiro, S., Cacho, I., Thouveny, N., Larrasoaña, J.C., Diez, S., Dañobeitia, J.J., 2006. Characterizing Holocene Paleoseismic Record in the SW Portuguese Margin. *Geophys. Res. Abstracts* 8, 08469.
- Vött, A., Brückner, H., Handl, M., Schriever, A., 2006. Holocene palaeogeographies of the Astakos coastal plain (Akarnania, NW Greece). *Palaeogeog., Palaeoclimatol., Palaeoecol.* 239, 126–146.
- Wagner, B., Bennike, O., Klug, M., Cremer, H., 2007. First indication of Storegga tsunami deposits from East Greenland. *J. Quat. Sci.* 22, 321–325.
- Whitehouse, U.G., Jeffrey, L.M., Debrecht, J.D., 1960. Differential settling tendencies of clay minerals in saline waters. *Clays Clay Min.*, 7th Natl. Conf, pp. 1–80.
- Yll, R., Zazo, C., Goy, J.L., Pèrez-Obiol, R., Pantaleón-Cano, J., Civis, J., Dabrio, C.J., González, A., Borja, F., Soler, V., Lario, J., Luque, L., Sierro, F., González-Hernández, F. M., Lezine, A.M., Deneffe, M., Roure, J.M., 2003. Quaternary palaeoenvironmental changes in south Spain. In: Ruiz Zapata, M.B., Dorado, M., Valdeolillos, A., Gil, M.J., Bardaji, T., Bustamante, I., Martínez, I. (Eds.), *Quaternary Climatic Changes and Environmental Crises in the Mediterranean Region*. Universidad de Alcalá, Ministerio de Ciencia y Tecnología, INQUA. Alcalá de Henares, pp. 201–214.
- Yokoyama, Y., Tezer, M.E., Lambeck, K., 2001. Coupled climate and sea-level changes deduced from Huon Peninsula cora terraces of the last ice age. *Earth Plan. Sci. Lett.* 193, 579–587.
- Zazo, C., Goy, J.L., Hillaire-Marcel, C., Dabrio, C.J., Belloumini, G., Improta, S., Lario, J., Bardaji, T., Silva, P.G., 1994. Holocene sequence of sea-level fluctuations in relation to climatic trends in the Atlantic–Mediterranean linkage coast. *J. Coast. Res.* 10, 933–945.
- Zazo, C., Dabrio, C.J., González, A., Sierro, F.J., Yll, E.J., Goy, J.L., Luque, L., Pantaleón-Cano, J., Soler, V., Roure, J.M., Hoyos, M., Borja, F., 1999. The record of the alter glacial and interglacial periods in the Guadalquivir marshlands (Mari López drilling, S. W. Spain). *Geogaceta* 26, 119–122.
- Zong, Y., Lloyd, J.M., Leng, M.J., Yim, W.W.-S., Huang, G.M., 2006. The reconstruction of Holocene monsoon history from the Pearl River Estuary, using diatoms and carbon isotope ratios. *The Holocene* 16, 251–263.